CSL COORDINATED SCIENCE LABORATORY

LEVEL II

ADA 085891

ELECTRICAL PROPERTIES AND PHOTOLUMINESCENCE OF GERMANIUM-IMPLANTED GALLIUM ARSENIDE

SIU-SING CHAN

DTIC
SELECTE
JUN 20 1980
S D
E

DDC FILE COPY

UNIVERSITY OF ILLINOIS – URBANA, ILLINOIS

80 6 17 0 20

REPORT DOCUMENTATION PAGE	READ INSTRUCTIONS BEFORE COMPLETING FORM

1. REPORT NUMBER	2. GOVT ACCESSION NO. AD-A085 191	3. RECIPIENT'S CATALOG NUMBER Masters thesis,

4. TITLE (and Subtitle) ELECTRICAL PROPERTIES AND PHOTOLUMINESCENCE OF GERMANIUM-IMPLANTED GALLIUM ARSENIDE.	5. TYPE OF REPORT & PERIOD COVERED Technical Report
	6. PERFORMING ORG. REPORT NUMBER R-872, UILU-ENG-80-2204

7. AUTHOR(s) Siu-Sing Chan	8. CONTRACT OR GRANT NUMBER(s) N00014-76-C-0806, N00014-79-C-0424

9. PERFORMING ORGANIZATION NAME AND ADDRESS Coordinated Science Laboratory University of Illinois at Urbana-Champaign Urbana, Illinois 61801	10. PROGRAM ELEMENT, PROJECT, TASK AREA & WORK UNIT NUMBERS 53

11. CONTROLLING OFFICE NAME AND ADDRESS Office of Naval Research; Joint Services Electronics Program	12. REPORT DATE Dec 79
	13. NUMBER OF PAGES 47

14. MONITORING AGENCY NAME & ADDRESS(if different from Controlling Office)	15. SECURITY CLASS. (of this report) UNCLASSIFIED
	15a. DECLASSIFICATION/DOWNGRADING SCHEDULE

16. DISTRIBUTION STATEMENT (of this Report)

Approved for public release; distribution unlimited

17. DISTRIBUTION STATEMENT (of the abstract entered in Block 20, if different from Report)

18. SUPPLEMENTARY NOTES

19. KEY WORDS (Continue on reverse side if necessary and identify by block number)

Ion Implantation
Germanium in Gallium Arsenide
Amphoteric Properties

20. ABSTRACT (Continue on reverse side if necessary and identify by block number)

The data presented show that Ge-implanted GaAs has a complex amphoteric behavior which is controlled by the implantation dose, implantation temperature and anneal temperature. Annealing was performed with r.f. plasma deposited Si_3N_4 as the encapsulant. Implantations at -100°C resulted in p-layers while those performed at 100°C and above resulted in n-layers regardless of the dose and anneal temperature. Room temperature implants resulted in p- or n-layers depending on the combination of dose and anneal temperature. Electrical acti-

20.

vation and carrier mobilities in the implanted layers were low. Low temperature (6 K) photoluminescence indicated that a significant amount of residual damage remained after annealing. Carrier concentration profiles in implanted layers and junction characteristics of Ge-implanted GaAs planar diodes are also presented.

ELECTRICAL PROPERTIES AND PHOTOLUMINESCENCE
OF GERMANIUM-IMPLANTED GALLIUM ARSENIDE

by

Siu Sing Chan

Accession For		
NTIS GRA&I		☑
DDC TAB		☐
Unannounced		☐
Justification		
By		
Distribution/		
Availability Codes		
Dist	Avail and/or special	
A		

ELECTRICAL PROPERTIES AND PHOTOLUMINESCENCE
OF GERMANIUM-IMPLANTED GALLIUM ARSENIDE

by

SIU SING CHAN

B.S., University of Illinois, 1976

THESIS

Submitted in partial fulfillment of the requirements
for the degree of Master of Science in Electrical Engineering
in the Graduate College of the
University of Illinois at Urbana-Champaign, 1980

Thesis Advisor: Professor B. G. Streetman

Urbana, Illinois

ELECTRICAL PROPERTIES AND PHOTOLUMINESCENCE
OF GERMANIUM-IMPLANTED GALLIUM ARSENIDE

by

Siu Sing Chan
Coordinated Science Laboratory

ABSTRACT

The data presented show that Ge-implanted GaAs has a complex
amphoteric behavior which is controlled by the implantation dose, implan-
tation temperature and anneal temperature. Annealing was performed with
r.f. plasma deposited Si_3N_4 as the encapsulant. Implantations at -100°C
resulted in p-layers while those performed at 100°C and above resulted in
n-layers regardless of the dose and anneal temperature. Room temperature
implants resulted in p- or n-layers depending on the combination of dose
and anneal temperature. Electrical activation and carrier mobilities in
the implanted layers were low. Low temperature (6°K) photoluminescence
indicated that a significant amount of residual damage remained after
annealing. Carrier concentration profiles in implanted layers and junction
characteristics of Ge-implanted GaAs planar diodes are also presented.

ACKNOWLEDGEMENTS

TABLE OF CONTENTS

1. INTRODUCTION

Germanium is known to be an amphoteric dopant in GaAs when it is introduced during crystal growth. Liquid-phase epitaxial (LPE) growth from Ga-rich Ge-doped solutions around 900°C results in p-layers [1,2]. Although the formation of n-layers were also reported by Kressel et al. [3] by varying the amount of Ge in the growth solution, their results have been contradicted by Rosztoczy et al. [2]. With vapor-phase epitaxial (VPE) methods, n-layers are obtained [4]. Using molecular-beam epitaxy (MBE), Ge is incorporated as an acceptor if the substrate surface is Ga-stabilized during growth, while it is incorporated as a donor if the substrate surface is As-stabilized [5].

Even in the cases when Ge-doping results in n-type conductivity, photoluminescence has revealed the presence of a Ge-associated acceptor level [4,5]. This suggests that Ge goes into both Ga and As sites in all cases, and the overall conductivity type is determined by the relative availability of the two kinds of crystal vacancies under a given set of growth conditions. In addition, there are indications that besides introducing simple donor and acceptor levels in GaAs, Ge also introduces deeper levels in the bandgap [2,3], which may be diatomic Ge complexes with lattice vacancies [6].

Ion implantation into GaAs produces large numbers of Ga and As vacancies. From the foregoing discussion, it should be interesting to study the electrical and photoluminescence properties of Ge-implanted GaAs and their relation to lattice vacancies introduced by ion bombardment. Some work along this line has been done by Zelevinskaya and Kachurin [7], and Ge was reported to be an n-type dopant. However, only low energy (30 keV) and relatively high dose implants were examined, and the subsequent annealing was done with silicon dioxide encapsulation at temperatures

up to only 700°C. The low implantation energy and the high ion doses resulted in very high concentrations of Ge within less than 500 Å of the sample surface. Moreover, the annealing temperature was too low to allow optimal recovery of the crystal structure, and SiO_2 is an ineffective encapsulant against Ge outdiffusion during annealing.

It is the purpose of this work to investigate more extensively the electrical properties and photoluminescence of Ge-implanted GaAs. Implantations are done at higher energies at a variety of substrate temperatures. Annealing is carried out at higher temperatures with silicon nitride encapsulation, which is a much better mask against Ga outdiffusion.

2. EXPERIMENTAL PROCEDURES

2.1. Implantation

Ion implantation has become a common technique for introducing impurities into semiconductors. It is used in preference to diffusion whenever high reproducibility, tight line-width, and impurity profile control are desired. The technique essentially consists of producing a plasma containing the desired impurity ions, extracting the ions with a high voltage, selecting the desired ions with an appropriate magnetic field, and directing them onto the target. The stopping processes which determine the distribution of the implanted ions in the substrate is described by the theory of Lindhard, Scharff, and Schiott (LSS) [8,9]. The stopping powers of the various elements comprising the substrate (a particular element designated as k) are each characterized by two parameters: its nuclear stopping power $S_{N,k}(E)$ and its electronic stopping power $S_{e,k}(E)$, which are functions of the incident ion energy E. The spatial rate of energy dissipation is given by

$$\frac{dE}{dx} = -\sum_k N_k [S_{N,k}(E) + S_{e,k}(E)]$$

where N_k is the concentration of the kth type of substrate element. An ion comes to rest when its energy becomes zero. The total distance R travelled is given by

$$R = \int_0^E \frac{dE}{\sum_k N_k [S_{N,k}(E) + S_{e,k}(E)]}$$

However, the quantity of interest is usually the distance travelled perpendicular to the substrate surface, or the projected range R_p. Since the interaction of the incident ions with the substrate is essentially

random in nature, there will be a spread in their distribution described by a standard deviation ΔR_p. The distribution profile in the LSS theory can be approximated by a Gaussian function

$$N(x) = \frac{N_{\square}}{\Delta R_p \sqrt{2\pi}} \; exp \left[- \frac{(x-R_p)^2}{2\Delta R_p^2} \right]$$

where $N_{\square}$ is the total number of implanted ions per unit surface area of the substrate, i.e., the implantation dose or fluence. The peak of the concentration distribution is

$$N_p = \frac{N_{\square}}{\Delta R_p \sqrt{2\pi}} \; \simeq \; \frac{0.4 N_{\square}}{\Delta R_p}$$

Values of R_p and ΔR_p according to the LSS theory for various ion/substrate combinations at various ion energies have been computed and tabulated [9].

The implantations in this work were performed with an Accelerators, Inc. model 300-MP ion implanter. GeH_x^+ (x=0,1,2,3,4) ions were produced by ionizing germane (GeH_4) in a hot cathode, and were implanted into GaAs substrates at an energy of 250 keV. The hydrogen attached to the Ge ions should dissociate and outdiffuse from the substrate during subsequent annealing, and was not considered in this work. All substrates were tilted 7° from the ion beam normal to avoid channelling effects. Provisions were made to heat or cool the substrates during implantation if necessary. Substrates for hot implants were protected by 200 Å - 300 Å of rf plasma deposited silicon nitride (see next section) prior to implantation.

The implantation was performed into either semi-insulating or n-type GaAs in this work. For Hall effect measurements, semi-insulating Cr-doped GaAs substrates were used, since it could not be known ahead of

time whether the implanted layer would be n-type or p-type. The semi-insulating nature of the substrate eliminated the need of a p-n junction to isolate the implanted layer from the substrate. For diode fabrication (with a Ge-implanted p-side) and photoluminescence, n-type (n $\sim 10^{15} cm^{-3}$) VPE GaAs layers on n$^+$ substrates were used.

2.2. Encapsulation and Annealing

To restore the structure of the crystal after implantation and to place the Ge atoms on electrically active lattice sites, the implanted material was thermally annealed at temperatures from 700°C to 900°C. Since unprotected GaAs dissociates at these temperatures [10], the implanted material was encapsulated with silicon nitride prior to the heat treatment to prevent surface degradation.

The effectiveness of oxygen-free Si_3N_4 films against Ga and As outdiffusion has been well established [11]. The apparatus for depositing the silicon nitride films used in this work is shown schematically in Fig. 2.1. The samples to be encapsulated were placed on a carbon strip in a pyrex reaction chamber, which was evacuated to $3x10^{-6}$ Torr with a diffusion pump system. Ultra-high purity N_2 was admitted into the chamber from the top at the rate of 50 standard cc per minute (sccm). A retractable stainless steel shutter was used to cover the samples, and an rf plasma was initiated and sustained for 1 min. The purpose of the preliminary N_2 plasma is to remove the last traces of oxygen in the chamber and ad-sorbed on its walls as oxides of nitrogen, which are then pumped out by the mechanical pump. A 2% mixture of SiH_4 in ultra-high purity argon was admitted at a rate of 11 sccm into the chamber through the gas dis-persing ring immediately above the samples and the shutter was retracted.
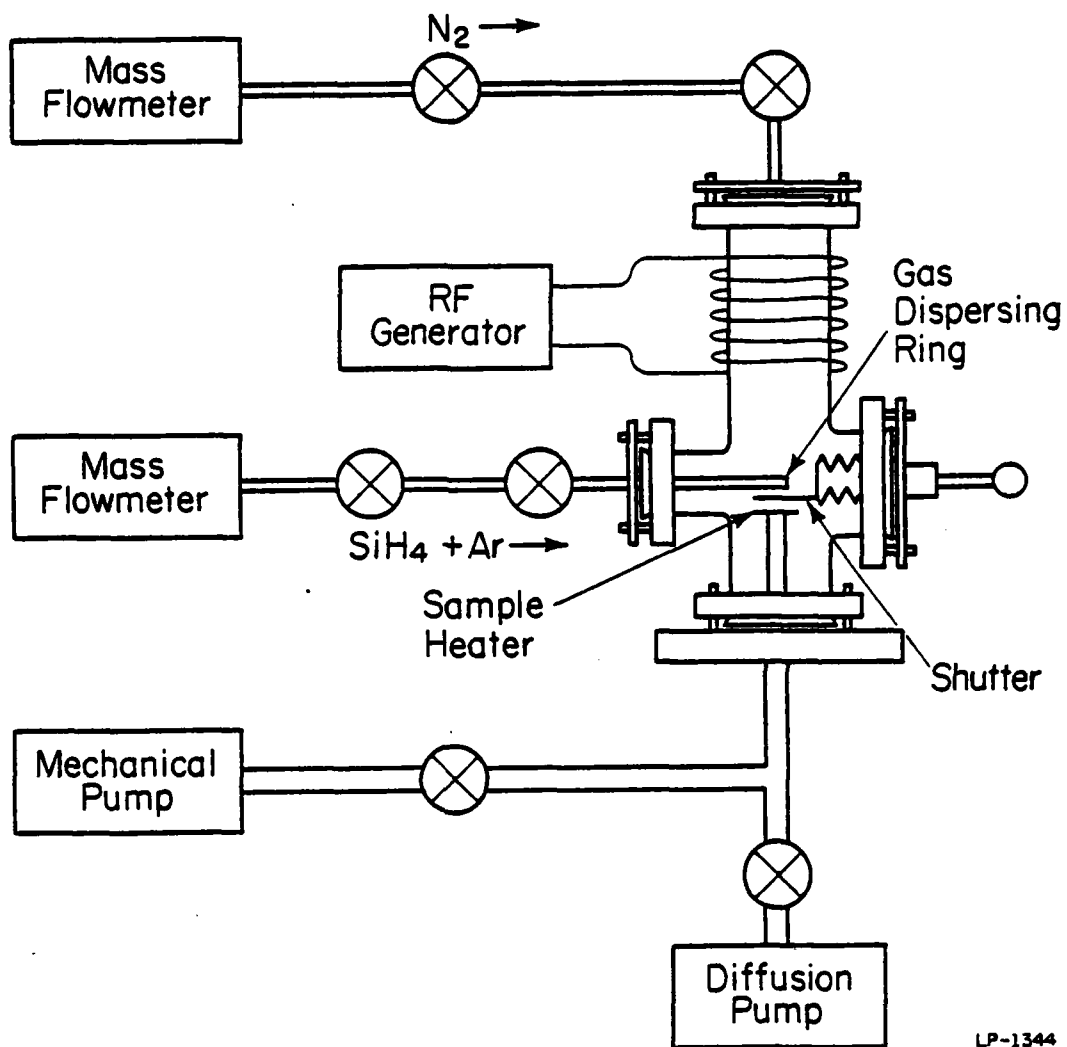
Fig. 2.1. Schematic diagram of the rf-plasma Si_3N_4 deposition system [25].

Current ($\sim$ 90 A) was passed through the carbon strip to raise its temp-
erature rapidly to 320°C, and the rf plasma was again initiated. Excited
nitrogen atoms in the plasma carried downwards by the gas flow reacted
with the SiH_4 in the vicinity of the gas dispersing ring to form silicon
nitride, which was then deposited on the heated samples.

The deposition rate as well as the Si:N atomic ratio of the
films are functions of the gas flow rates [12]. The flow rates used here
were chosen to result in stoichiometric silicon nitride (Si:N atomic ratio =
0.75) [12]. Typical film thickness used were approximately 1000 Å, and
the deposition times were approximately 15 min.

Thermal annealing was done in a 12" TransTemp gold-coated tube
furnace. The samples were placed in a clean silica liner, and a stream of
forming gas (4% H_2 in ultra-high purity N_2) was maintained over the samples.
All anneals were 30 min. in duration.

2.3. Resisitivity and Hall Effect Measurements

2.3.1. Sample Preparation

The most convenient geometry for resistivity and Hall effect
measurements is the van der Pauw geometry [13], in which the sample is a
disc of arbitrary shape with four ohmic contacts at arbitrary points on
its periphery. In this work the van der Pauw geometry was approximated
by a clover-leaf pattern.

Upon removal of the silicon nitride encapsulant after annealing,
a square array of four contact pads was evaporated onto each sample
through a shadow mask. For p-type implanted layers, the contact metal
was a Ag-Mn alloy (96% Ag, 4% Mn) [14]. For n-type layers, a Au-Sn alloy
(96% Au, 4% Sn) was used. The contacts were annealed in a hydrogen

atmosphere for 30 sec. Annealing temperatures were 350°C and 400°C for
Ag-Mn and Au-Sn contacts, respectively.

By mounting the samples face down on an appropriate stainless
steel mask with glycol phthalate, grooves were made between contact pads
with an abrasive air jet in a configuration as shown in the inset of Fig.
2.2. Since the implanted layers were less than a micron deep, the grooves
made in this fashion always extend into the semi-insulating substrate. Thus
the contact pads were electrically isolated from one another except through
the central region of the sample among the four grooves. Since the interior
ends of the grooves were very close together, this central region might
be considered as a van der Pauw disc, with the contact pads connected by
short strips of the implanted layer to its periphery.

Each sample was then mounted with an insulating varnish
(Ge 7031) on a nylon disc, which fitted into a nylon sample holder (Fig. 2.2).
The sample was positioned on the disc such that the contact pads made
contact with four non-magnetic spring-loaded "pogo-stick" probes. A notch
in the nylon disc fitted onto a locking pin in the sample holder so that
the sample could be easily realigned with the "pogo-stick" probes in the
event that it had been removed from the holder and subsequently reinserted.
The sample holder could be inserted into a small solenoidal a.c. magnet
for double a.c. Hall measurements or between the poles of a permanent
magnet for d.c. Hall measurements.

This particular mounting scheme for the samples was designed to
facilitate repetitive resistivity and Hall effect measurements in conjunc-
tion with successive layer removal, to yield a profile of electrically
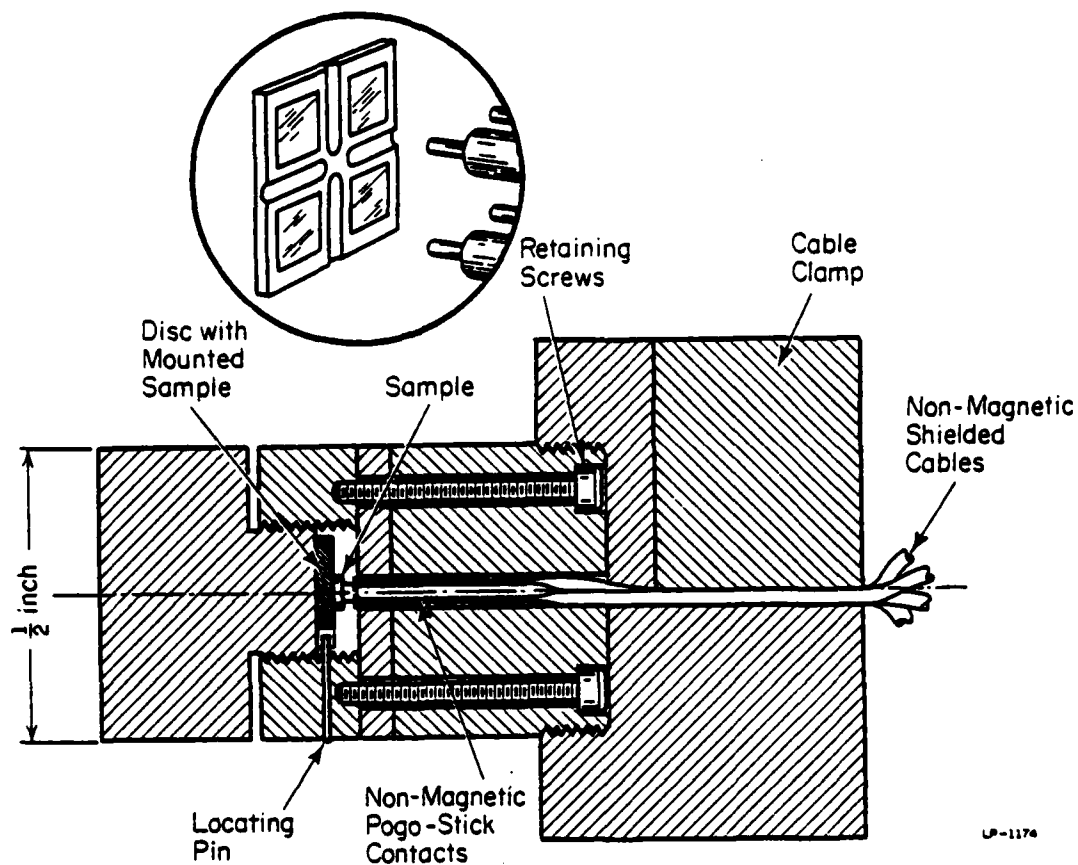active Ge. Layer removal was accomplished with a chemical etch consisting

Fig. 2.2. Cross-sectional view of the sample holder used for van der Pauw
resistivity and Hall measurements. The inset shows the sample
geometry and the spring-loaded contacts in the holder [16].

of equal parts of electronic grade conc.H_2SO_4 and 30% H_2O_2 diluted with
an appropriate amount of deionized water. The etch rate and hence the
thicknesses of the removed layers were monitored by protecting small
regions of the samples near the edges with black Apiezon wax and measuring the
resulting step heights with a Sloan Dektak mechanical stylus.

Etch rates of Ge-implanted GaAs were found to vary widely, de-
pending probably on the residual damage in the sample. A typical etch
rate of a 1:1:300 etch mixture on a sample implanted at room temperature
was 200 Å/min. The etch rate for a 1:1:200 mixture on samples implanted
at 200°C was about 800 Å/min, while the etch rate for the same mixture
on a sample implanted at room temperature and annealed with SiO_2 was
about 350 Å/min.

2.3.2. Double a.c. Method [15]

With the van der Pauw geometry and d.c. excitation, the Hall
voltage appears as a small correction to a large background voltage upon
the application of the magnetic field, rendering it difficult to measure
with good accuracy. The difficulty is further complicated by various
thermoelectric and misalignment effects which must be averaged out by
permutation of field and current.

In the double a.c. method, the current and magnetic field are
driven at well-separated frequencies. The Hall voltage occurs at the
heterodyne frequencies, and can be measured with phase lock-in techniques
with excellent sensitivity and noise rejection. As a result, only small
magnetic fields (several hundred gauss) are necessary. Permutation of
field and current is carried out automatically, and hence only one meas-
urement is necessary. The double a.c. method is therefore very convenient

and well suited for electrical profiling, where small changes in the Hall
voltage must be detected repeatedly as surface layers are removed by
chemical etching.

By their very nature, voltages in resistivity measurements
occur at the same frequency as the current excitation.

A block diagram of the double a.c. Hall system used in this
work is shown in Fig. 2.3 [15]. A circuit schematic is also included
(Fig. 2.4) [16]. The sample current was driven by oscillator f_1 at a
frequency of 1 kHz. The 200 gauss (rms) solenoidal magnet was driven by
oscillator f_2 and a power amplifier at a frequency of 250 Hz. The resis-
tivity voltages occurred at 1 kHz and the Hall voltage was detected at
$f_1 - f_2 = 750$ Hz. These signals were measured by a PAR 186A lock-in
amplifier. The reference signal for the measurement of the Hall voltage
was generated from oscillators f_1 and f_2 with a mixer and a three-stage
tuned active filter.

In practice it was found that the resistivity voltages could
be measured accurately with great ease, while the Hall voltage was some-
times noisy, especially if the sample was resistive. The noise was sub-
tracted out by taking the difference of the readings with the samples in
and out of the magnetic field.

2.3.3. D. C. Method

One drawback of the a.c. method is that it does not yield
convenient information about the majority carrier type in the sample. Al-
though the phase of the double a.c. Hall voltage is usually a good indi-
cation of the majority carrier type, a d.c. Hall measurement is helpful
for confirmation.

Fig. 2.3. Block diagram of the double a.c. Hall system [16].

Fig. 2.4. Circuit diagram of the double a.c. Hall system [16].

13
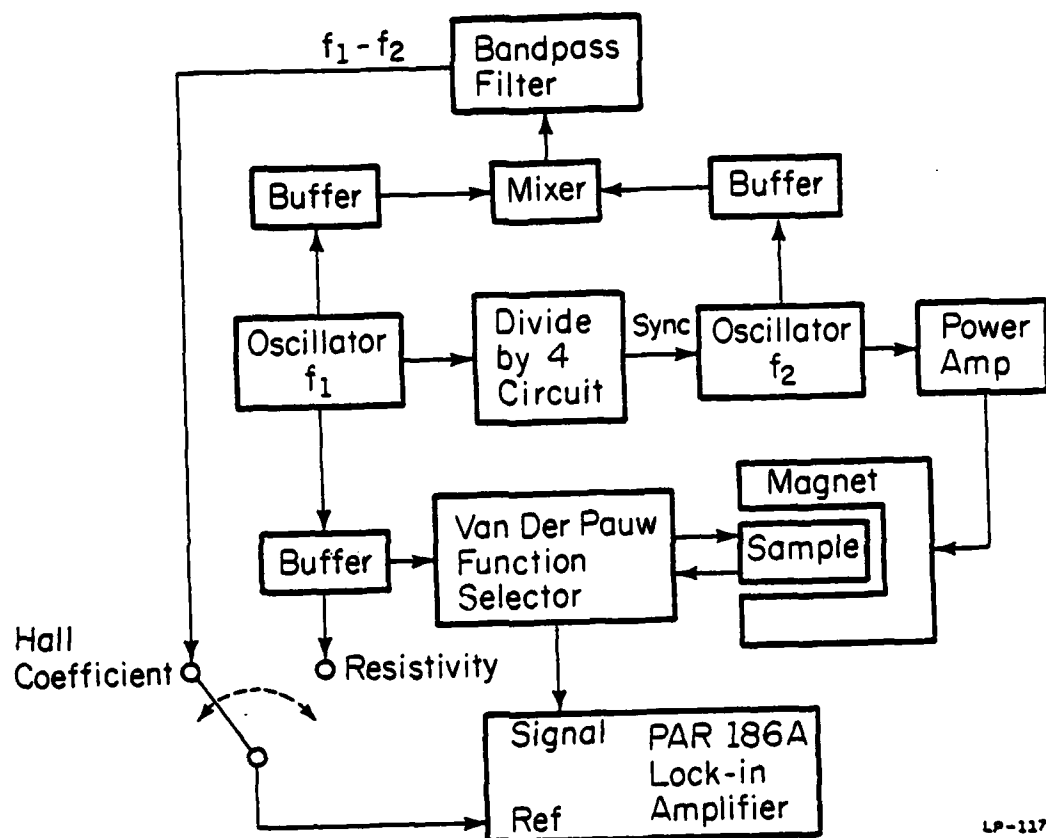
D.C. Hall measurements were made with a 2500 gauss permanent magnet using the same van der Pauw geometry and sample holder as in the double a.c. case. Each measurement was repeated with the current reversed to eliminate field misalignment effects. The polarity of the Hall voltage was then compared with that of a Be-implanted GaAs sample, which was known to be p-type. Although usually only the polarity of the Hall voltage was of interest, d.c. resistivity measurements were also made for comparison with the double a.c. data.

2.3.4. Data Analysis

Resistivity and Hall measurements in conjunction with layer removal furnish information concerning the carrier concentration and mobility at various depths in the implanted layer. With a van der Pauw geometry and the double a.c. approach, the sheet resistivity ρ and sheet Hall coefficient R_H of the implanted layer are given by [13]

$$\rho = \frac{\pi}{\ln 2} \left(\frac{R_{ABCD} + R_{BCDA}}{2}\right) \quad f \quad \left(\frac{R_{ABCD}}{R_{BCDA}}\right)$$

$$R_H = \frac{\sqrt{2} \ \Delta R_{BDAC}}{B_o(\text{rms})}$$

Labeling the contacts on the sample consecutively by A, B, C and D, R_{ABCD} is defined by

$$R_{ABCD} = \frac{V_{CD}}{I_{AB}}$$

where V_{CD} is the voltage of contact D over that of contact C due to a current I_{AB} entering the sample at contact A and leaving at contact B. Similarly R_{BCDA} and ΔR_{BDAC} are defined by

$$R_{BCDA} = \frac{V_{DA}}{I_{BC}}$$

$$\Delta R_{BDAC} = \frac{\Delta V_{AC}}{I_{BD}}$$

The voltages associated with R_{ABCD} and R_{BCDA} are related to resistivity and are therefore measured at the same frequency as the current. The voltage ΔV_{AC} associated with ΔR_{BDAC} is the Hall voltage due to the magnetic field B_0 and is measured at the difference (heterodyne) frequency. The function $f(R_{ABCD}/R_{BCDA})$ has been tabulated by van der Pauw [13].

For d.c. measurements, the expression for ρ is unchanged. However, the sheet Hall coefficient becomes

$$R_H = \frac{\Delta R_{BDAC}}{B_0(d.c.)}$$

Assuming that the Hall coefficient factor due to various scattering mechanisms is approximately unity, the average mobility μ and sheet carrier concentration N_s in the implanted layer are given by

$$\mu = \frac{R_H}{\rho}$$

$$N_s = \frac{1}{qR_H}$$

where q is the electronic charge.

If ρ_j, $R_{H,j}$ are the values of ρ and R_H before a layer of thickness d_j is removed from the implanted layer and ρ_{j-1}, $R_{H,j-1}$ are the corresponding values after etching, the average mobility μ_j and average carrier concentration n_j in the removed layer are given by [17]

$$\mu_j = \frac{R_{H,j}}{\rho_j} + \frac{R_{H,j-1}}{\rho_{j-1}} - \frac{R_{H,j-1} - R_{H,j}}{\rho_{j-1} - \rho_j}$$

$$n_j = \frac{\frac{1}{\rho_j} - \frac{1}{\rho_{j-1}}}{qd_j\mu_j}$$

Again, the Hall coefficient factor has been assumed to be 1. The error associated with this assumption is probably less significant than the experimental uncertainties [16].

2.4. Planar Diode Fabrication

It has been shown that planar GaAs p-n junctions with high breakdown voltages and extremely low leakage currents can be fabricated with beryllium implantation and annealing with silicon nitride encapsulation [18]. It is therefore desired to investigate the corresponding properties of Ge-implanted junctions.
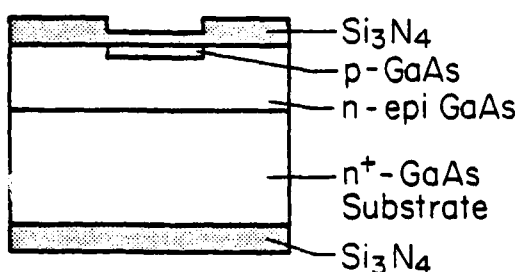
The planar process for fabricating diodes is outlined in Fig. 2.5. The starting material was lightly-doped n-type (n $\sim 10^{15}$ cm^{-3}) VPE GaAs on an n$^+$ substrate. The Ge-implantation dose and the subsequent annealing temperature were chosen such that the implanted layer would be p-type. The implantation mask was AZ 1350 positive photoresist. To delineate the implanted regions from the rest of the surface, a layer of Si$_3$N$_4$ (~ 700 Å) was deposited on the front surface of the GaAs before the photoresist was applied. The photoresist pattern was duplicated in the Si$_3$N$_4$ layer by etching in HF. After implantation, the photoresist was removed and the sample was annealed with more Si$_3$N$_4$ encapsulation. Upon removal of the encapsulant from the back surface, Ag-Sn contacts were formed on the n$^+$ substrate by evaporation through a shadow mask and annealed for 30 sec. at
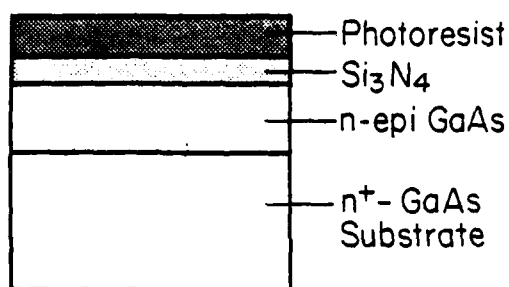
Photoresist — Encapsulate sample with
Si_3N_4 — Si_3N_4 and apply photoresist.
n-epi GaAs

n^+- GaAs
Substrate
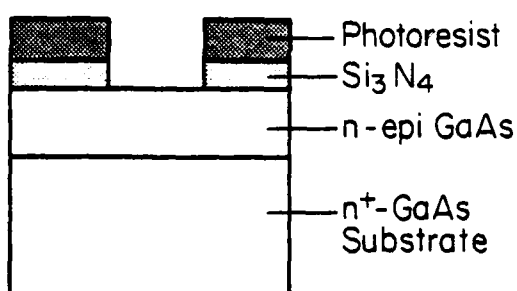
Photoresist — Expose PR with a suitable
Si_3N_4 — mask, develop and open
n-epi GaAs — windows in Si_3N_4.
Ion implant Ge.

n^+-GaAs
Substrate

Si_3N_4 — Strip photoresist, encapsulate
p-GaAs — with Si_3N_4 and anneal.
n-epi GaAs

n^+-GaAs
Substrate

Si_3N_4
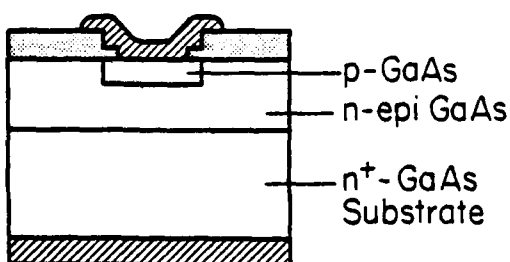
Evaporate Ag-Sn for back contact.
p-GaAs — Open front contact windows,
n-epi GaAs — evaporate and define Ag-Mn
contacts.

n^+-GaAs
Substrate

LS-1380

Fig. 2.5.   Planar process for Ge-implanted p^+-n GaAs diodes [22].

350°C in hydrogen. Photoresist processes were then used to open contact windows in the front nitride layer and define Ag-Mn contacts to the implanted regions. The Ag-Mn contacts were annealed under the same conditions as Ag-Sn contacts. The back contacts were processed first to avoid excessive heat treatment of the front contacts.

Junction characteristics were measured with a Keithley 225 current source and a Keithley 610 CR electrometer.

2.5. Photoluminescence

Low temperature photoluminescence is a very sensitive technique to study the amount of residual damage in the lattice and the various radiative centers introduced by impurities and defects in the bandgap. By optically exciting the samples with photons having an energy larger than the bandgap, excess carriers are generated near the surface. These will tend to diffuse into the bulk of the sample and recombine via various radiative and non-radiative processes. For highly damaged samples, the non-radiative processes dominate and the resulting light emission will be weak. The spectral distribution of the emitted light will reveal the energy levels of radiative centers and estimates of their relative abundances. A good review of the theoretical and experimental aspects of photoluminescence has been documented by Bebb and Williams [19,20].

Since the absorption length of the incident photons is a function of their energy, the position of the peak of the excess carrier distribution is dependent upon the wavelength of the excitation. As a general rule, the position of the peak is nearer to the sample surface for shorter wavelength excitations. To investigate the true state of the implanted layer, it should ideally coincide with the peak of the impurity distribution.

According to LSS range statistics [9], the peak of the Ge distribution

for 250 keV implants into GaAs occurs at approximately 900 Å from

the surface.

In this work, the excitation source was the 4579 Å line from a

Coherent Radiation Model 52G Argon-Krypton laser. The absorption length

of this line in GaAs is approximately 770 Å [21], and the peak of the

excess carrier distribution is estimated to be at 1500 Å from the surface.

The position of this peak may actually be even closer to the surface if

the crystal contains a high density of recombination centers due to

residual damage. The samples maintained around 6°K in a Janis "Super

Varitemp" liquid helium cryostat. The spectra of the emitted light were

analyzed by a Jarrel-Ash 1/2 meter scanning spectrometer and detected

with an S-1 photomultiplier and a PAR HR-8 lock-in amplifier. A sche-
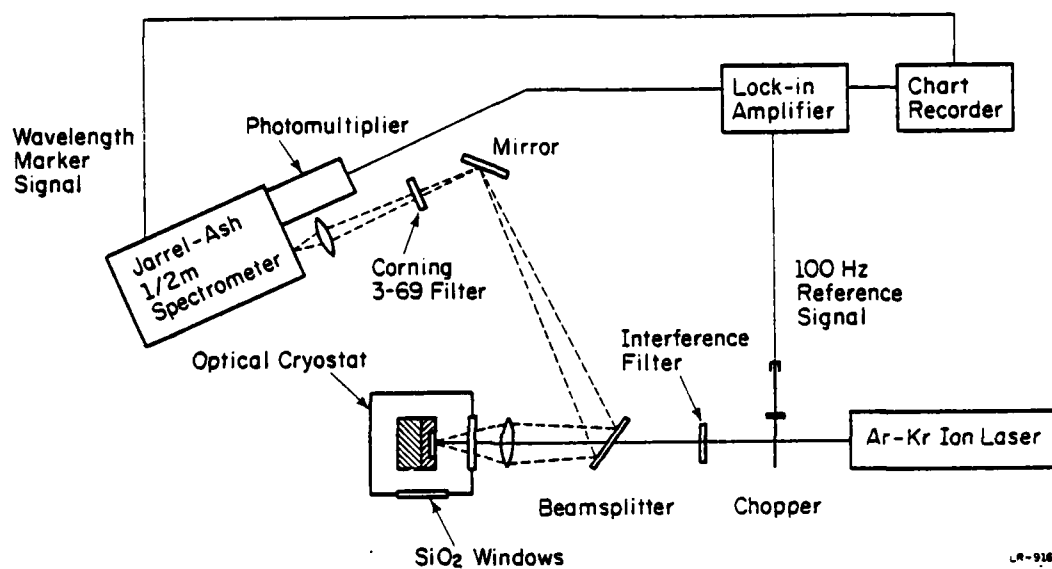
matic diagram of the set-up is shown in Fig. 2.6.

Fig. 2.6. Schematic diagram of the photoluminescence apparatus [16].

3. RESULTS AND DISCUSSION

Previous studies by glow discharge optical spectroscopy (GDOS) [22] of the atomic distribution of implanted Ge in GaAs showed that the atomic profile before annealing is closely approximated by LSS range statistics. After annealing at 900°C with Si_3N_4 encapsulation, some diffusion occurs but the atomic profile is still reasonably localized (Fig. 3.1). The results of the present work furnish complementary information of the electrical and optical activity of the implanted Ge.

3.1. Electrical Activation and Carrier Mobility

Implantations have been done at doses of 10^{13}, 10^{14} and 10^{15} ions/cm^2. For each dose, implantations were repeated with substrates at -100°C, room temperature, 100°C and 200°C. Samples from each implant were annealed at 750°C, 800°C and 850°C. Anneal temperatures below 750°C were found to result in very little electrical activity, presumably because of insufficient lattice recovery at these temperatures. A single pair of double a.c. resistivity and Hall measurements was used to determine the sheet carrier concentration and average mobility in each implanted layer. The majority carrier type was determined by a d.c. Hall measurement. The results are summarized in Figs. 3.2-3.4.

Substrates implanted at -100°C were found to be p-type regardless of dose and anneal temperature. On the contrary, substrates implanted at 100°C and 200°C were always n-type. However, substrates implanted at room temperature exhibit a dose-dependent amphoteric behavior. Ion doses of 10^{13} and 10^{15} cm^{-2} result in n-type layers for all anneal temperatures, but ion doses of 10^{14} cm^{-2} result in p-layers for annealing temperatures of 750°C and 800°C. In addition, attempts to make ohmic contacts with
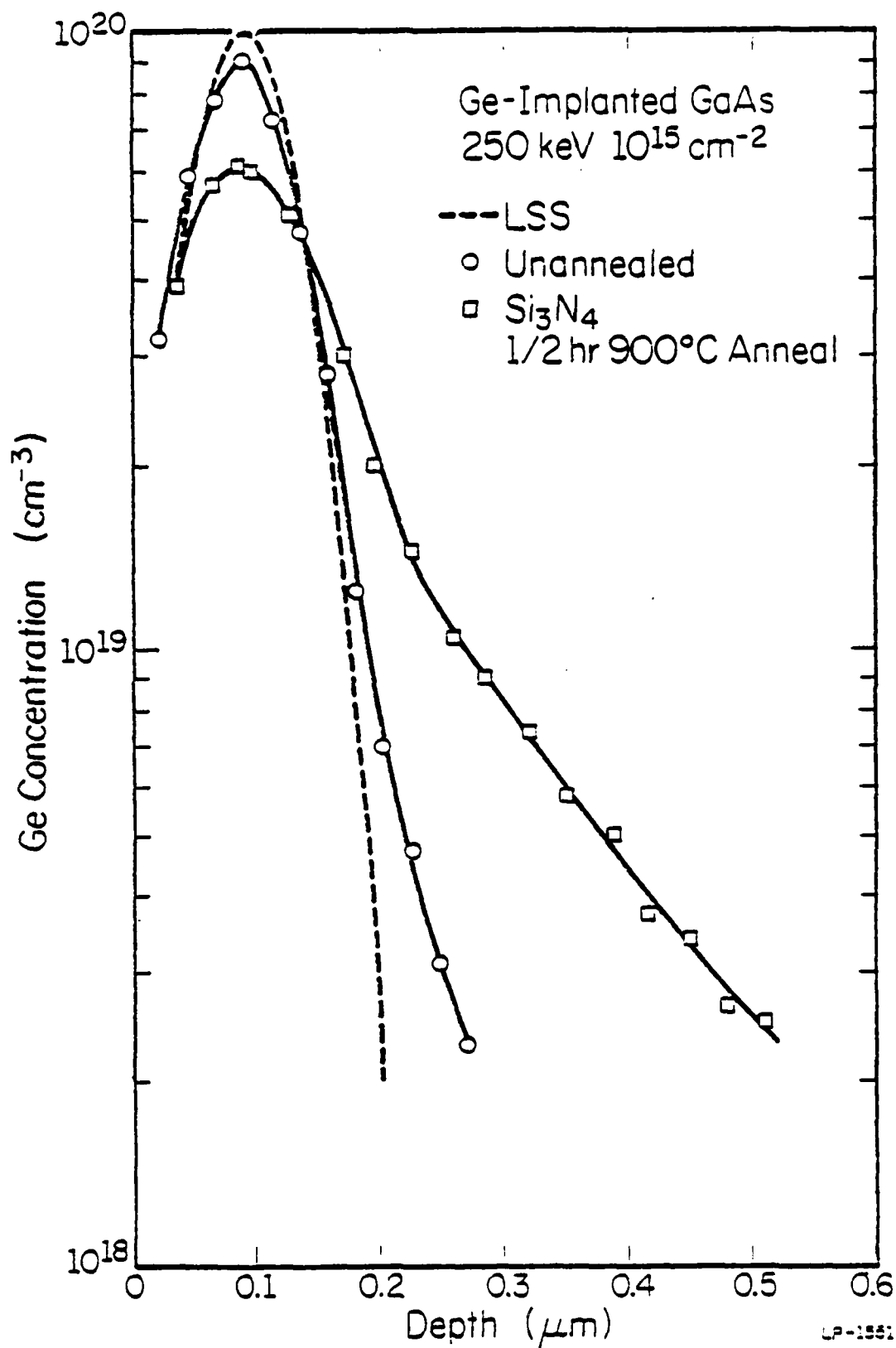
Fig. 3.1. GDOS profiles of the atomic Ge distributions before and after a 1/2 hr. anneal at 900°C using Si₃N₄ encapsulation.

Fig. 3.2.   Sheet carrier concentrations and average carrier mobilities due
to 10^{13} ions/cm^2 Ge implants as functions of the anneal temper-
ature and implantation temperature.

Fig. 3.3. Sheet carrier concentrations and average carrier mobilities due to 10^{14} ions/cm² Ge implants as functions of the anneal temperature and implantation temperature.

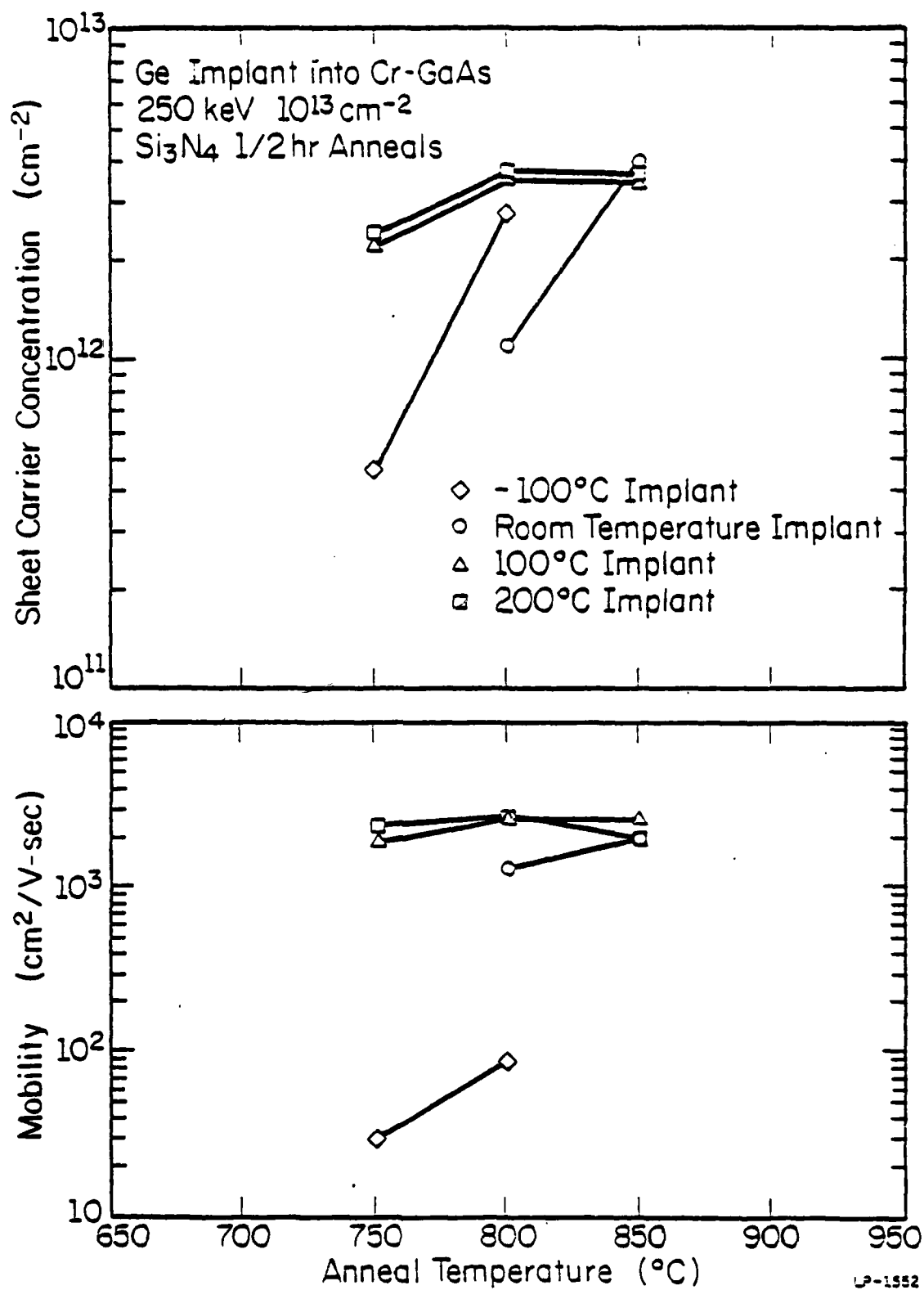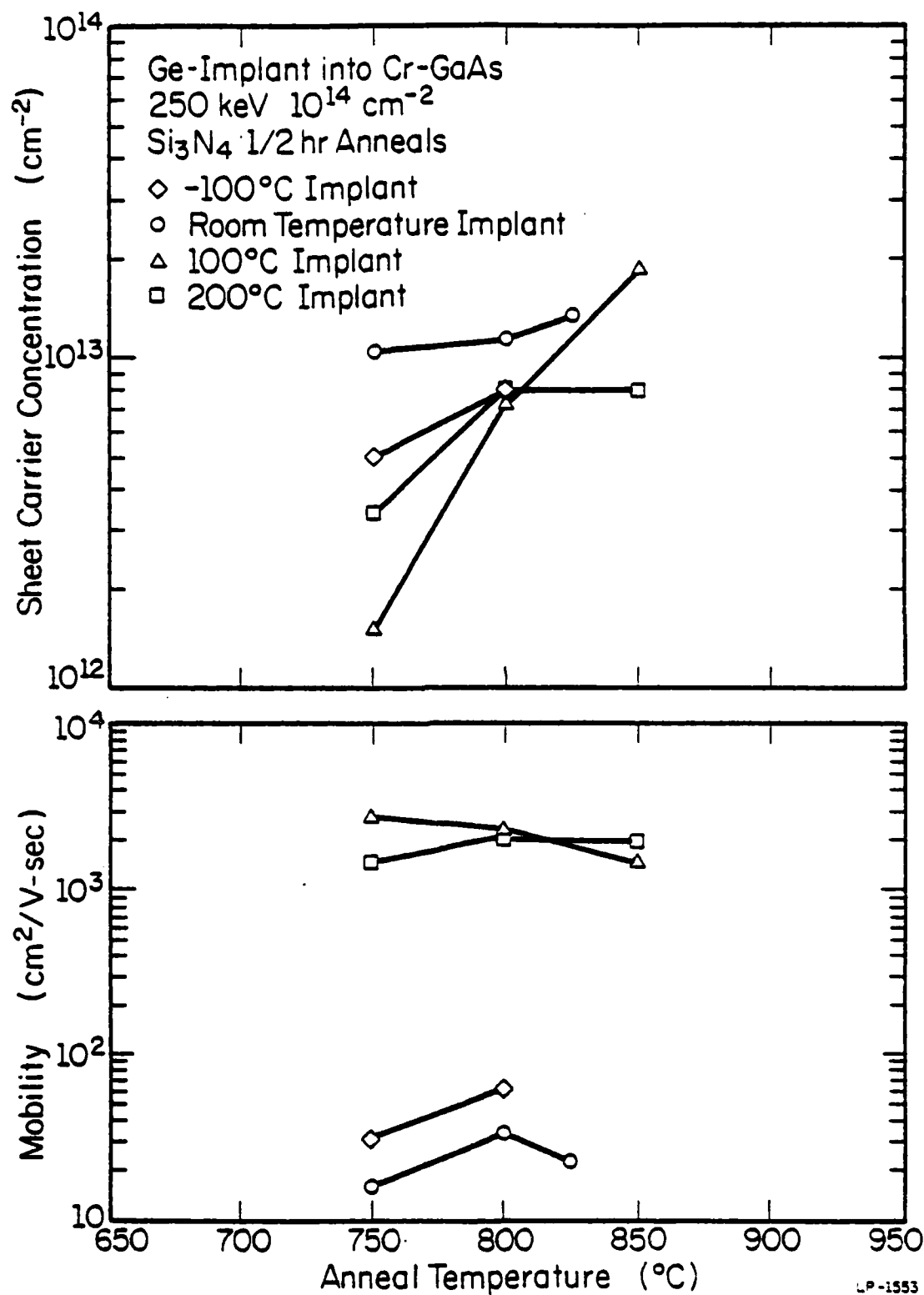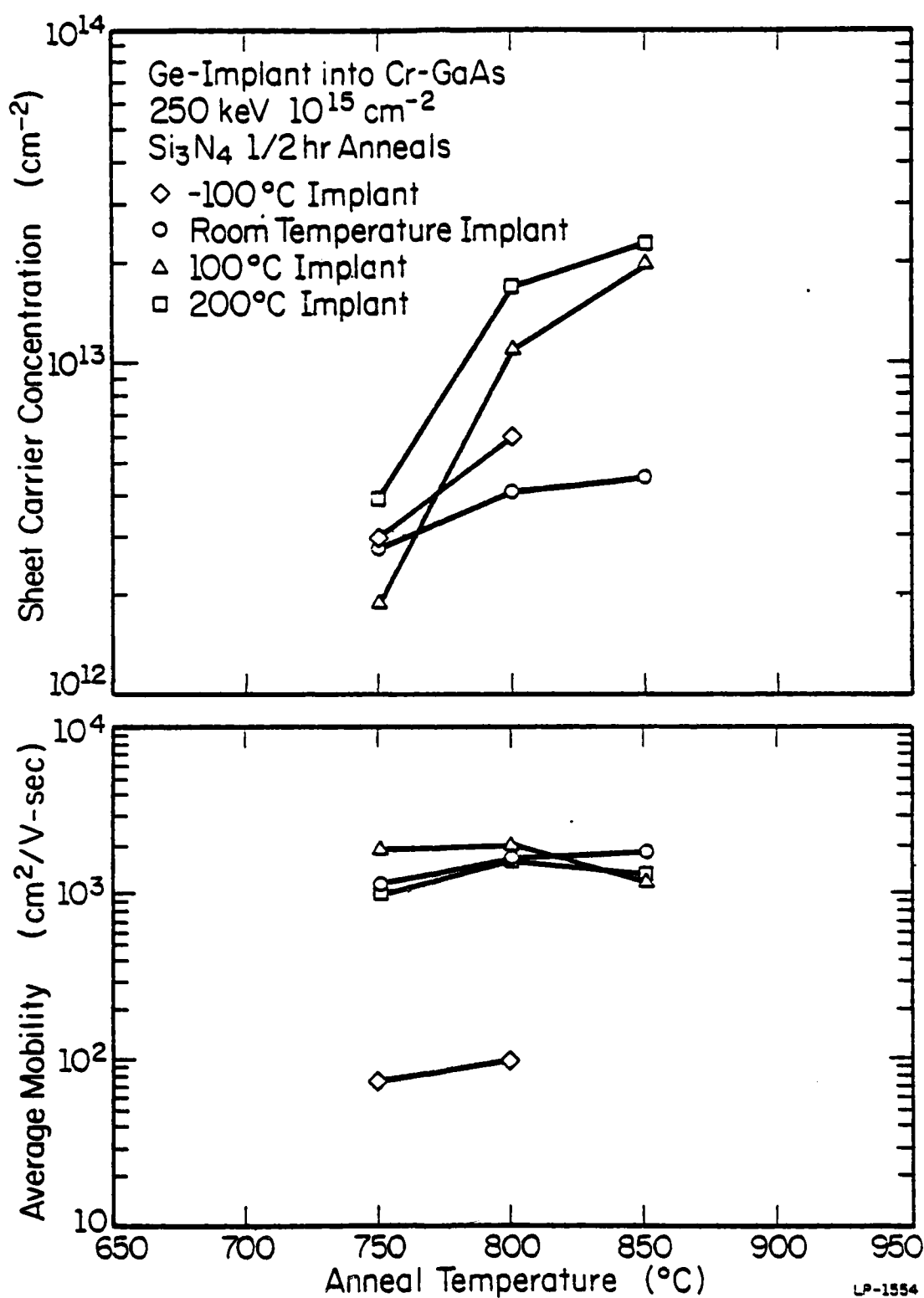Fig. 3.4. Sheet carrier concentrations and average carrier mobilities due to 10^{15} ions/cm² Ge implants as functions of the anneal temperature and implantation temperature.

either Ag-Mn or Au-Sn to these samples (dose = 10^{14} ions/cm^2) failed if they were annealed at 850°C. This indicates that a conductivity type conversion, similar to that reported by Marcyk [22] when SiO$_2$ is used as the encapsulant, might be starting at around 850°C. The same samples annealed at 825°C were p-type.

To further investigate the range of doses for which the anneal temperature has an effect on the amphoteric behavior of the implanted Ge, room temperature implants at the intermediate doses of 5×10^{13} and 5×10^{14} ions/cm^2 were done. It was found that the 5×10^{13} ions/cm^2 implant resulted in an annealing behavior which exhibited a definite conversion from p- to n-type at 850°C (Fig. 3.5). No contact-making problem was encountered with samples annealed at 850°C in this case. The annealing behavior of the 5×10^{14} ions/cm^2 implant was similar to that of a 10^{15} ions/cm^2 implant, i.e., n-type layers were formed for all anneal temperatures (Fig. 3.6).

The electrical activation of the implanted Ge was low, and was a function of the implantation and the anneal temperature. Generally speaking, for implantation doses of 10^{13} and 10^{15} ions/cm^2, at which the resulting majority carrier types were independent of the annealing temperature, the electrical activation increases with annealing temperature. For room temperature implantations and subsequent annealing at 800°C, the observed activations were 11%, 0.35% and 0.4% for doses of 10^{13}, 5×10^{14} and 10^{15} ions/cm^2 respectively. In these cases, raising the implantation temperature to 100°C had the effect of increasing the electrical activation by a factor of 3. However, the improvement leveled off quickly as the implantation temperature was further increased to 200°C. A 300°C

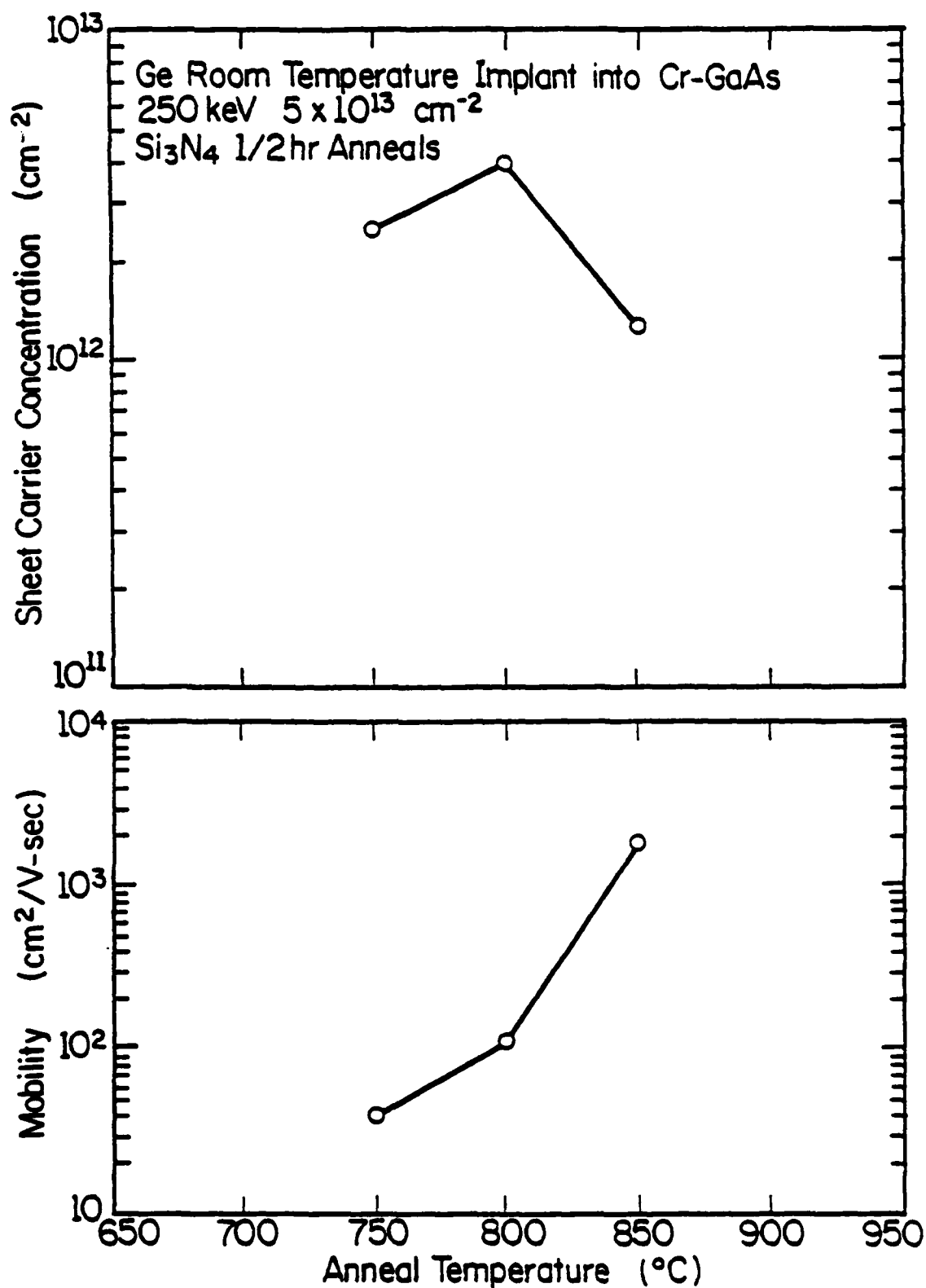Fig. 3.5. Sheet carrier concentrations and average carrier mobilities due
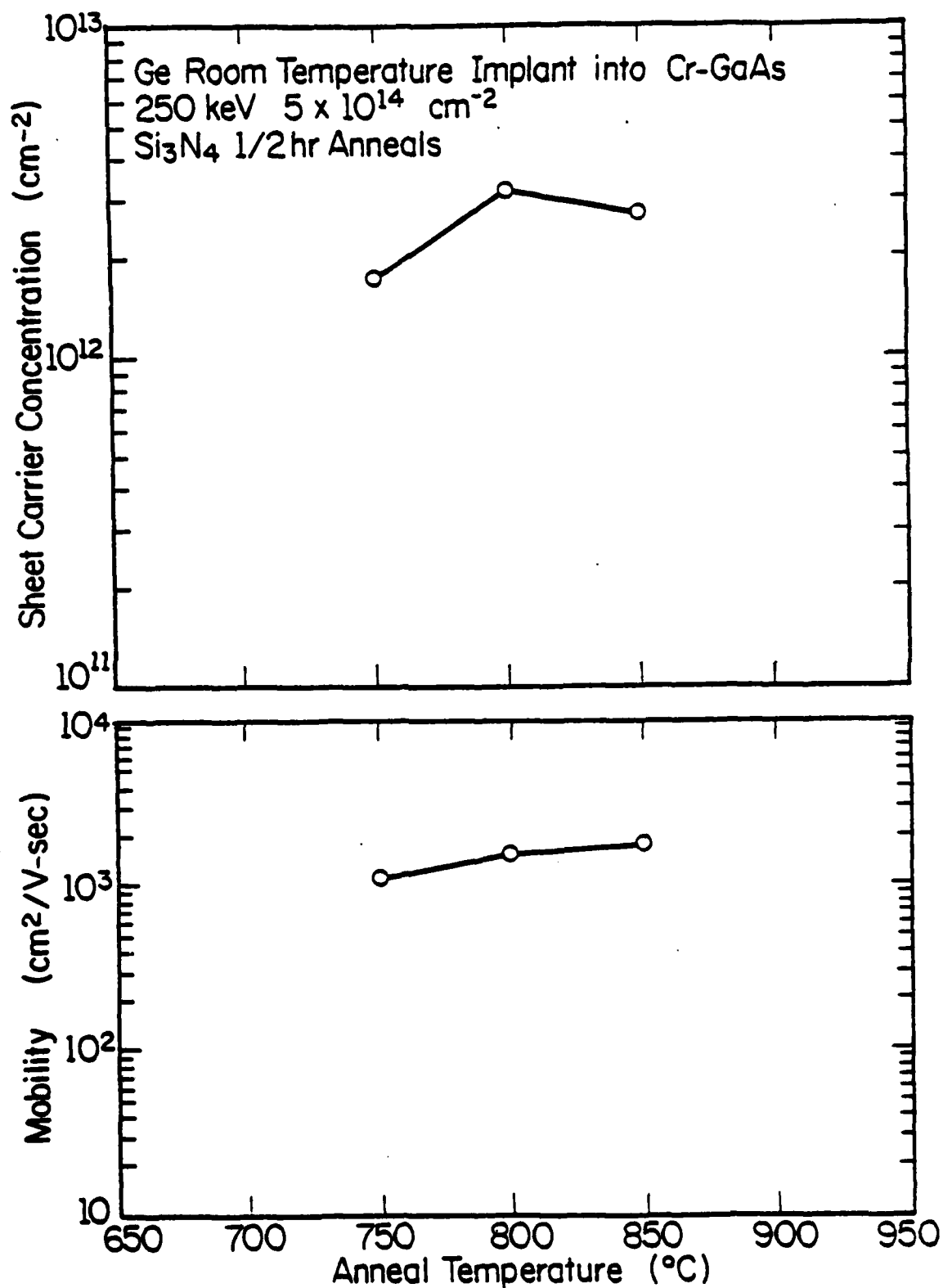to room temperature 5×10^{13} ions/cm^2 Ge implants.

Fig. 3.6. Sheet carrier concentrations and average carrier mobilities due to room temperature 5×10^{14} ions/cm^2 Ge implants.

implant was also done for the dose of 10^{15} ions/cm^2. The activation was essentially the same as the 200°C implant.

For room temperature implants at a dose of 5×10^{13} ions/cm^2, where the conductivity type was dependent on the anneal temperature, the p-type activation was 8% for 800°C anneals and dropped sharply to an n-type activation of 2.6% when the annealing temperature was raised to 850°C.

The observed carrier mobilities were low, ranging from 15 to 90 cm^2/V-sec for p-type layers and from 1000 to 2800 cm^2/V-sec for n-type layers. Implantation and anneal temperatures did not have significant effects on the carrier mobilities.

Since Cr-doped GaAs is known to lose its semi-insulating properties upon heat treatment above a certain temperature, and the hot implants were performed through thin (200 Å - 300 Å) Si$_3$N$_4$ layers, control experiments have to be performed to make sure (1) that the observed conductivity in the implanted layers was not due to changes in the substrate during annealing and (2) that the increased activation and exclusively n-type conductivity resulting from hot implants were not due to Si recoil implantation as the incident GeH$_x^+$ ions passed through the protective Si$_3$N$_4$ film. For these purposes, 250 keV, 200°C Ar$^+$ implants into Cr-doped GaAs substrates were performed at doses of 10^{13}, 10^{14} and 10^{15} ions/cm^2 in the presence of thin surface Si$_3$N$_4$ films. Samples from each implant were annealed under the same conditions as the Ge implants. No resulting conductivity was observed for anneal temperatures of 750°C and 800°C. Some p-type conductivity was found after annealing at 850°C for all three Ar$^+$ doses. Thus it can be concluded that Si recoil implantation effects, which will result in n-type conductivity, were negligible, and that the

substrate stayed semi-insulating up to 800°C. Since the substrate turned p-type after annealing at 850°C, data which showed that implanted layers were p-type after annealing at this temperature were not reliable. However, data which showed that the implanted layers were n-type at this anneal temperature were still qualitatively correct. For this reason, no sheet carrier concentration and mobility data are shown in Figs. 3.2-3.4 for this temperature in the case of -100°C implants.

In summary, implanted Ge in GaAs exhibits a complex amphoteric behavior which is a function of the implantation dose, implantation temperature and annealing temperature. This suggests that the electrical characteristics are controlled by the amount of lattice damage introduced during implantation and the amount of residual damage after annealing. To further investigate this possibility, room temperature Ar^+ implants at 250 keV were performed into Ge-doped expitaxial GaAs to introduce comparable amounts of damage as the Ge implants. For Ar^+ doses of 10^{13} and 10^{15} ions/cm^2, p-type Ge-doped LPE GaAs (p = 7.7×10^{16} cm^{-3}) was used as the implantation substrate. For Ar^+ doses of 10^{14} ions/cm^2, n-type Ge-doped MBE GaAs (n = 8.25×10^{17} cm^{-3}) was used. Annealing temperatures were 800°C and 850°C for the LPE samples and 800°C for the MBE samples. Since the corresponding Ge implants resulted in n-layers for doses of 10^{13} and 10^{15} ions/cm^2 and p-layers for doses of 10^{14} ions/cm^2, the object of the experiment was to observe whether the LPE samples converted to n-type and the MBE samples converted to p-type after the Ar^+ implantations and subsequent annealing. Contrary to expectations, no such type conversions took place. Hence, it seems that the amphoteric behavior of implanted

Ge is controlled by its concentration in conjunction with the amount of radiation damage.

3.2. Distribution Profiles of Electrically Active Ge

For Ge implants at 250 keV into GaAs, LSS range statistics predict a Gaussian distribution profile which is peaked at approximately 900 Å from the surface and has a standard deviation of approximately 400 Å [9]. It also predicts that for doses of 10^{13}, 10^{14} and 10^{15} ions/cm^2, the peak concentrations of Ge will be 10^{18}, 10^{19} and 10^{20} cm^{-3} respectively. Previous GDOS studies [22] have revealed the atomic distribution of implanted Ge before and after annealing, and in this work differential double a.c. Hall measurements have been used to study the distribution profiles of electrically active Ge after the annealing process.

Electrical profiles of room temperature and 200°C implants at doses of 10^{14} and 10^{15} ions/cm^2 are shown in Figs. 3.7 and 3.8. The room temperature implants are characterized by a surface inactive layer in which the carrier concentration is very low, and which is thicker in the higher dose implant. The corresponding carrier concentration profiles end very abruptly. The conducting layer is about 900 Å thick for the two doses shown. The peak hole concentration in the 10^{14} ions/cm^2 implant is approximately 3×10^{18} cm^{-3} while the peak electron concentration in the 10^{15} ions/cm^2 implant is approximately 5.5×10^{17} cm^{-3}.

Upon raising the implantation temperature to 200°C, the surface inactive layer largely disappeared for the 10^{14} ions/cm^2 implant. However, it is still present in the 10^{15} ions/cm^2 implant, although it has become thinner. The profiles do not end as abruptly as before, and are much more
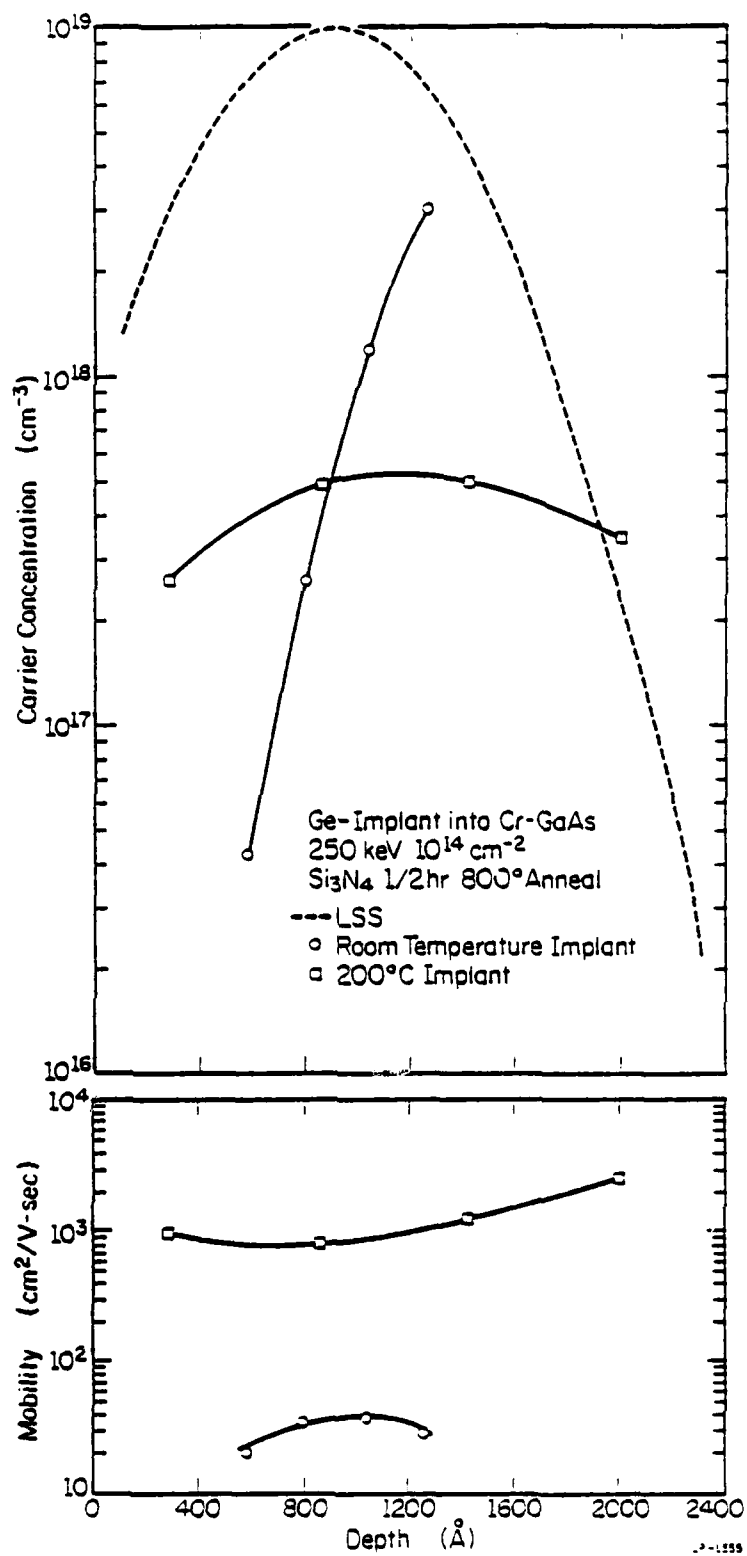
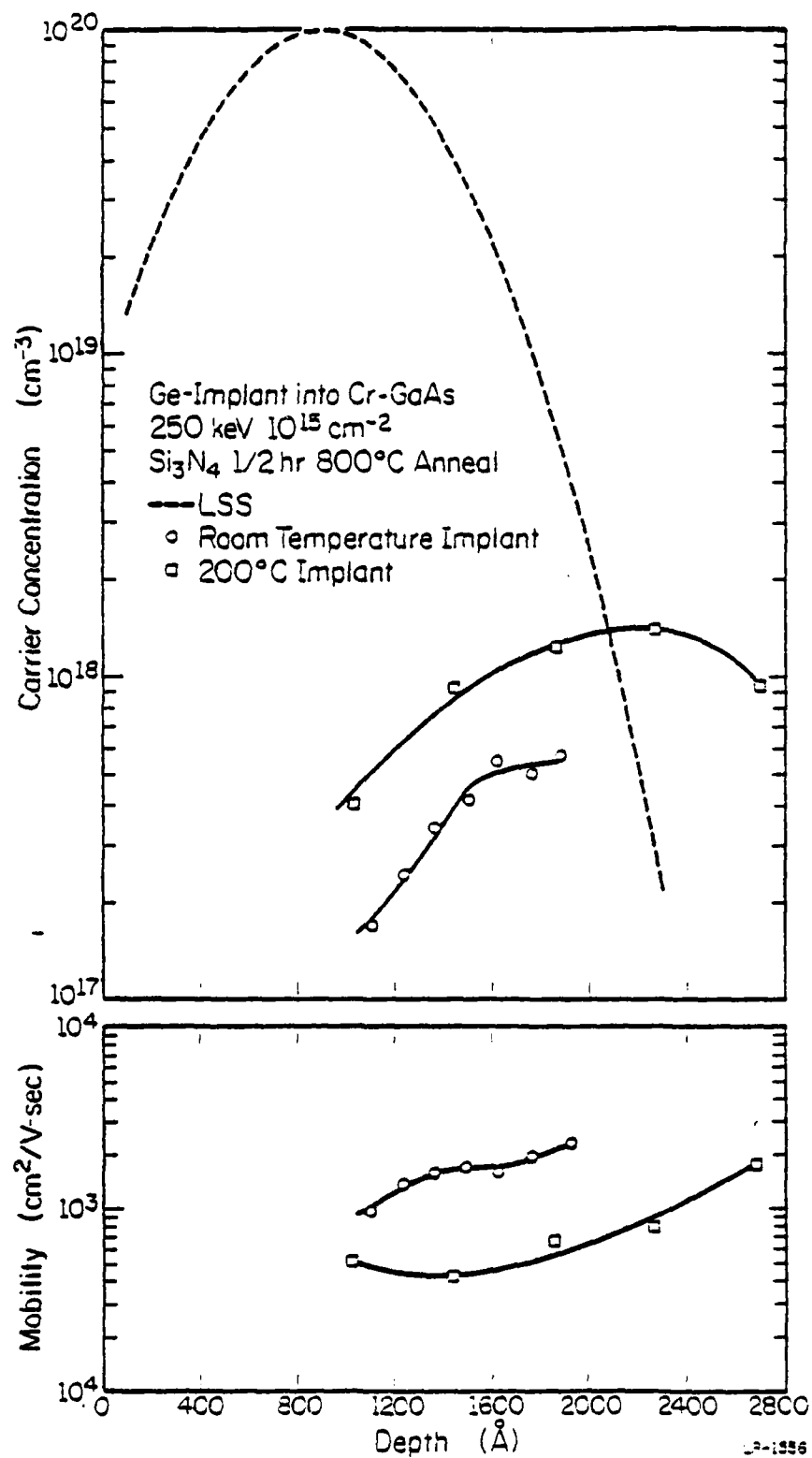Fig. 3.7 Carrier concentration and mobility profiles for 10^{14} ions/cm^2 Ge implants at room temperature and 200°C.

Fig. 3.8. Carrier concentration and mobility profiles for 10^{15} ions/cm^2
Ge implants at room temperature and 200°C.

spread out. The conducting layer is approximately 2000 Å thick in both cases. The peak electron concentrations are $\sim 5 \times 10^{17}$ cm^{-3} for the 10^{14} ions/cm^2 implant and $\sim 1.5 \times 10^{18}$ cm^{-3} for the 10^{15} ions/cm^2 implant.

The fact that the surface inactive layer is thicker for higher dose implants and can be reduced by heating the substrate during implantation suggests that it is a damaged region with a high density of defect-related carrier traps. Thus the crystal never fully recovers from the radiation damage and this may be a reason why the observed carrier mobilities are low.

There is an anomaly observed in the profiling process. The sum of the sheet carrier concentrations measured in the removed layers is very significantly larger than the total sheet carrier concentration measured in the implanted layer before etching was started. Also the carrier mobility in each of the removed layers is in many cases much lower than the average mobility measured in the original implanted layer.

3.3. Junction Characteristics

p^+-n diodes have been fabricated by performing a 10^{14} ions/cm^2 room temperature GeH_x^+ implant into n-type VPE GaAs (n $\simeq 10^{15}$ cm^{-3}) grown on an n^+ substrate. Subsequent annealing at 800°C resulted in a p^+ implanted layer. The forward and reverse junction characteristics are shown in Fig. 3.9.

The reverse breakdown is soft. An ohmic component of the reverse current dominates the leakage at reverse biases less than 2V. The leakage increases almost exponentially between 5V and 35V, and finally avalanches
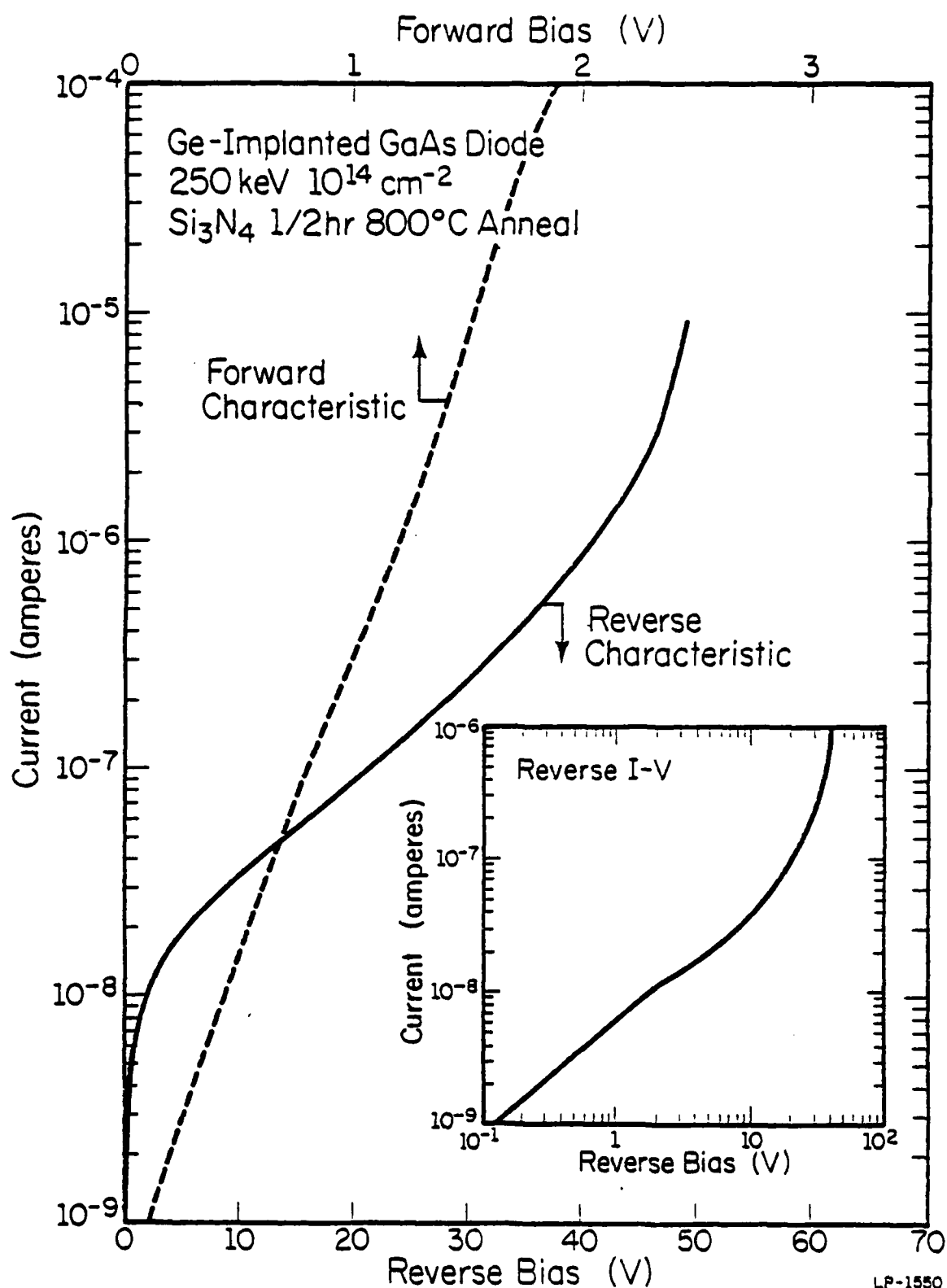
Fig. 3.9. Junction characteristics of Ge-implanted GaAs p^+-n planar diodes.
The inset shows the reverse characteristic on a log-log plot.

at 50V. The forward current is proportional to exp(qV/nkT), with an anomalous value of n = 6.2.

The ohmic component in the leakage current indicates the presence of a resistive shunt across the junction. Since electrical profiles reveal the formation of a surface inactive layer under the same implantation and annealing condition as have been used for the diodes, this suggests that the inactive layer is the source of the ohmic leakage. The exceptionally large value of n is intriguing and not understood.

3.4. Photoluminescence

Ge is known to introduce a low temperature photoluminescence peak at 1.481 eV when it is incorporated into GaAs during crystal growth [2,4]. The origin of this peak has been attributed to a band-to-Ge-acceptor transition [2,4]. By monitoring this peak as well as any additional peaks in the photoluminescence of Ge-implanted GaAs, additional information may be obtained which may help to explain the complex pattern of electrical activity.

VPE n-type GaAs (unintentionally doped, $n \simeq 10^{15}$ cm^{-3}) was used for implants for photoluminescence studies. Shown in Fig. 3.10 are the photoluminescence spectra of the unprocessed starting material, and, for purposes of comparison, those of p-type Ge-doped LPE GaAs (p = 7.7x10^{16} cm^{-3}) and n-type Ge-doped MBE GaAs (n = 4.2x10^{15} cm^{-3}, 3.67x10^{16} cm^{-3}, and 8.25x10^{17} cm^{-3}).

The spectrum for the unprocessed VPE material contains a peak at 1.515 eV which is attributed to free exciton recombination. There is also a small peak at 1.491 eV with a shoulder at 1.481 eV. The peak at
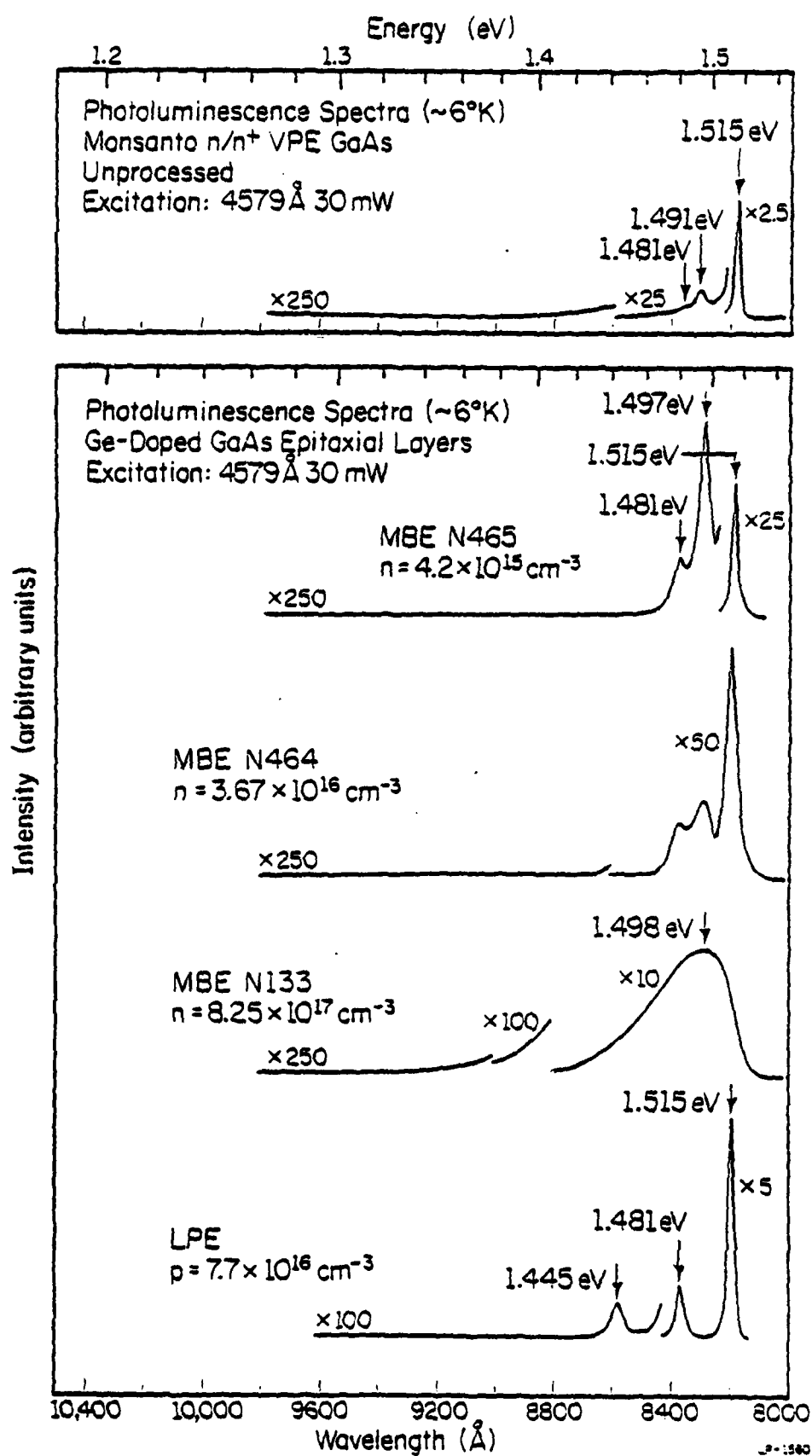
Fig. 3.10. Photoluminescence spectra of unprocessed VPE GaAs, n-type Ge-doped MBE GaAs and p-type Ge-doped LPE GaAs.

1.491 eV is probably due to Si, which may have been unintentionally introduced during VPE growth. The shoulder at 1.481 eV coincides in energy with the reported Ge-acceptor peak, and is of doubtful origin. However, its intensity is very small.

The spectrum for the p-type Ge-doped LPE sample contains the free exciton peak, the Ge-acceptor peak at 1.481 eV and its first LO phonon replica at 1.445 eV. The spectra for the two more lightly doped MBE samples (n = 4.2×10^{15} cm^{-3} and n = 3.67×10^{16} cm^{-3}) are similar. Each contains the free exciton peak, the Ge-acceptor peak and a third peak at 1.497 eV. This new peak is believed to be a band-to-acceptor peak associated with carbon, the presence of which is not uncommon in MBE material. For the MBE sample with n = 8.25×10^{17} cm^{-3}, there is only one very broad peak centered at 1.498 eV. Since the Ge-acceptor peak has been reported to broaden very considerably with increasing Ge-concentration [2], the broad peak at 1.498 eV is probably an overlap of the Ge-acceptor peak with the C-acceptor peak and the free exciton peak.

Fig. 3.11 shows the photoluminescence spectra of 10^{13} ions/cm^2 room temperature Ge-implants. The anneal temperatures range from 700°C to 900°C. The free exciton peak is the dominant feature of the spectra for all anneal temperatures. The intensity of this peak is a measure of the lattice recovery from radiation damage. Also present for all anneal temperatures are the Si-acceptor peak at 1.491 eV, the Ge-acceptor peak at 1.481 eV, and the peak at 1.360 eV associated with Ga-vacancies [23]. The peak at 1.325 eV for the 800°C, 850°C and 900°C anneals is believed to be the first LO phonon replica of the Ga-vacancy peak. The intensity of the free exciton peak is maximum for 850°C anneals, indicating optimum lattice
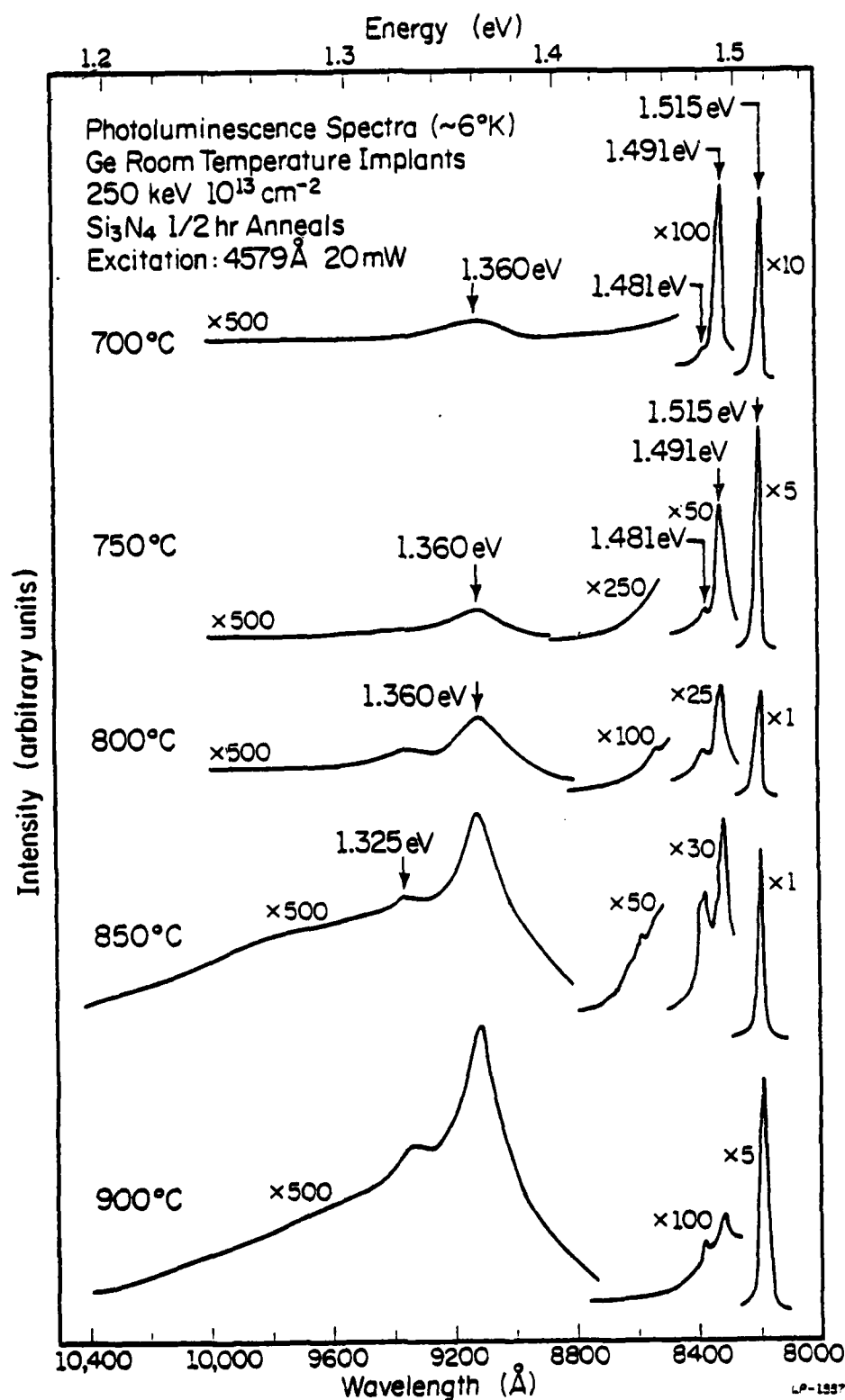
Fig. 3.11. Photoluminescence spectra of room temperature 10^{13} ions/cm^2
Ge implants annealed at various temperatures.

recovery at this temperature. However, the Ga-vacancy peak is also present for this and all other temperatures, meaning that the lattice never fully recovers. The intensity of the Si-acceptor peak relative to the free exciton peak is higher in all cases than in the unprocessed VPE material, showing that some Si indiffusion from the Si_3N_4 encapsulant may have taken place during annealing. The intensity of the peak at 1.481 eV increases both in magnitude and relative to the free exciton peak as the anneal temperature is raised from 700°C to 850°C, which confirms that it is indeed the Ge-acceptor peak and that more Ge is incorporated into electrically active sites at the higher anneal temperatures. As with the free exciton peak, the Ge-acceptor peak decreases in intensity as the anneal temperature is further raised to 900°C.

The features in the photoluminescence spectra (Fig. 3.12) of the 10^{14} ions/cm^2 implants are similar. The free exciton peaks are weaker than those for 10^{13} ions/cm^2 implants. Hence the degree of lattice recovery is even less. Again, lattice recovery and the incorporation of Ge into electrically active sites (as measured by the intensity of the Ge-acceptor peak) are maximum for samples annealed at 850°C. However, at this temperature a new peak appears at 1.432 eV. A peak at a similar energy, due to a deep acceptor level ($\sim$ 70 meV above the valence band) involving a Ge atomic complex, has also been reported by Kressel et al. for Ge-doped LPE GaAs [3]. However, their results have been contradicted by Rosztoczy et al. [2]. Upon raising the anneal temperature to 900°C for this ion dose, the Ge-acceptor peak and the Si-acceptor peak merge together to form a broad peak centered at 1.487 eV. In addition, an extremely broad peak
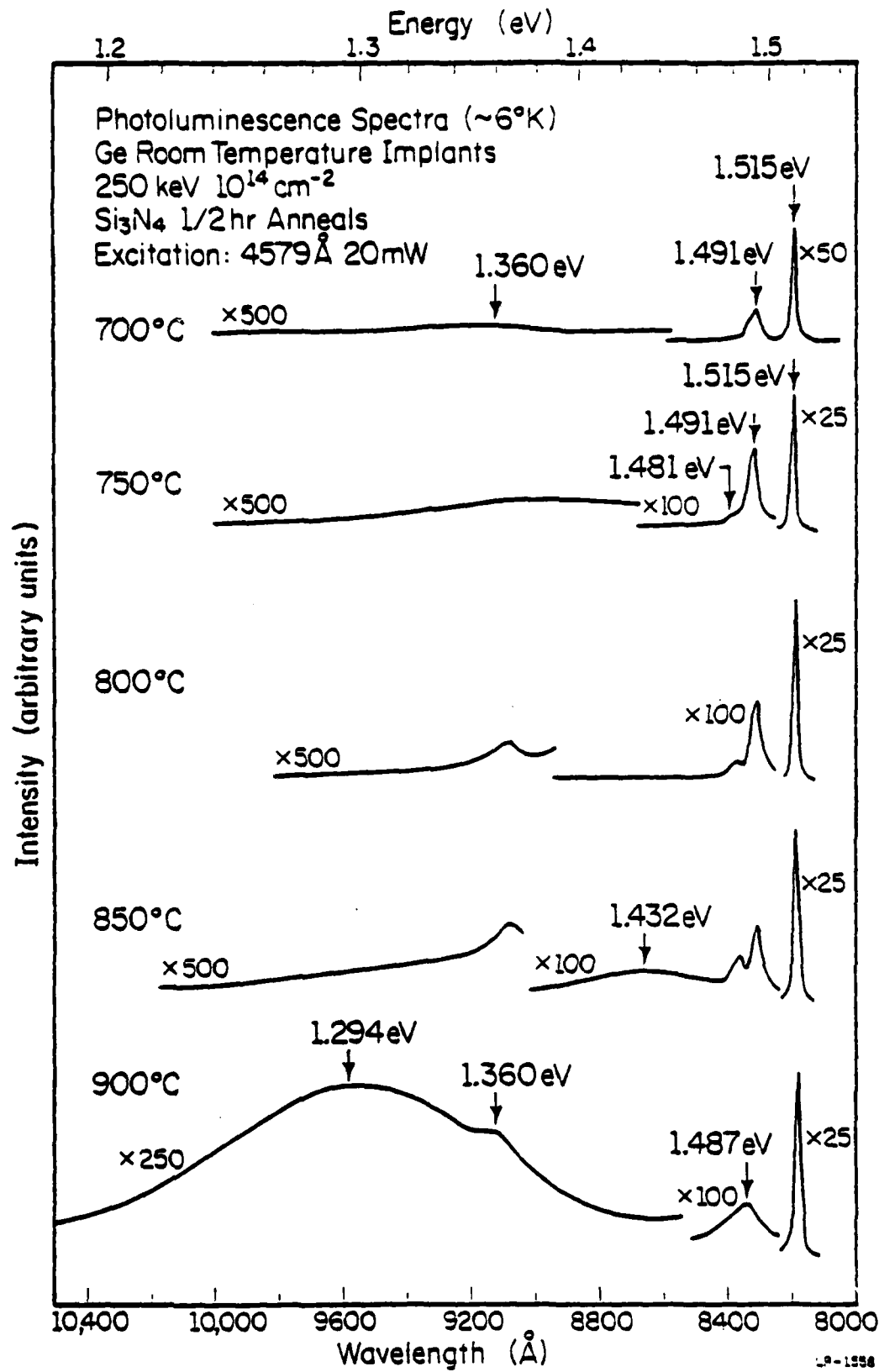
Fig. 3.12. Photoluminescence spectra of room temperature 10^{14} ions/cm^2 Ge implants annealed at various temperatures.

centered at 1.294 eV appears and overwhelms everything else. The origin of this peak is unknown.

Although the implanted layers are p-type for the dose of 10^{14} ions/cm^2 and annealing at no more than 800°C, the Ge-acceptor peaks in these cases are still very weak compared to the free exciton peaks. This is consistent with the low electrical activation observed in these layers, and is contrary to the behavior of Be implanted in GaAs, where the Be-acceptor peak is the dominant feature in the photoluminescence spectrum [24].

The photoluminescence spectra (Fig. 3.13) of the 10^{15} ions/cm^2 implants are exactly analogous to those of the 10^{13} ions/cm^2 implants, except that the intensities of the Ga-vacancy peaks are higher, while those of the other peaks are lower.
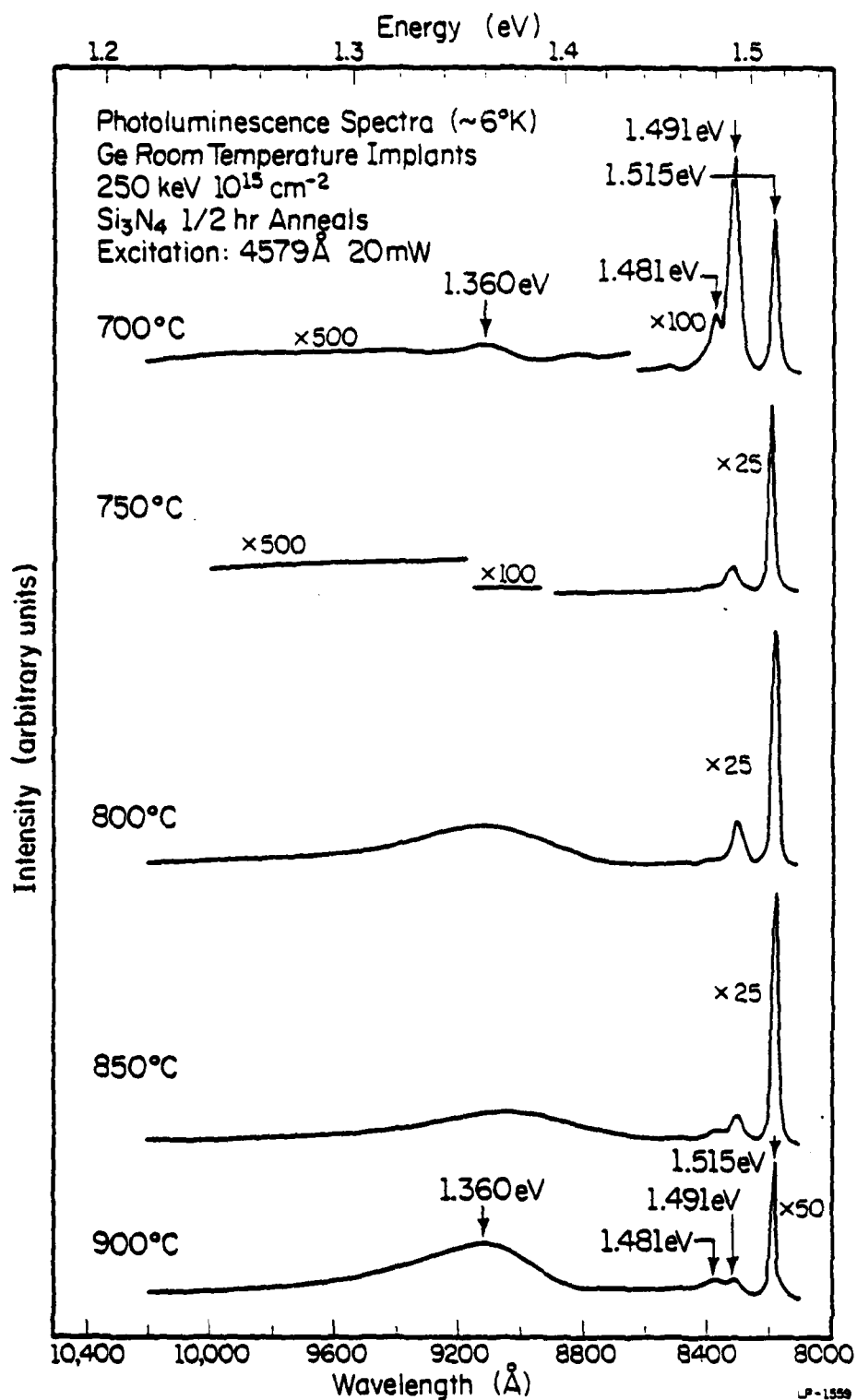
Fig. 3.13. Photoluminescence spectra of room temperature 10^{15} ions/cm^2 Ge implants annealed at various temperatures.

4. CONCLUSIONS

Ge implanted into GaAs has been demonstrated to be an amphoteric dopant whose behavior is controlled by the combined effects of implantation dose, implantation temperature and anneal temperature. For electrical measurements, implantation doses ranging from 10^{13} to 10^{15} ions/cm^2 and anneal temperatures ranging from 750°C to 850°C have been investigated. The implanted layers are always p-type when the implantation temperature is -100°C and they are always n-type when the implantation temperatures are 100°C and 200°C. For room temperature implants, n-layers are formed irrespective of the anneal temperature for doses of 10^{13}, 5×10^{14} and 10^{15} ions/cm^2. The intermediate doses of 5×10^{13} and 10^{14} ions/cm^2 result in p-layers if the anneal temperature is no more than 800°C. N-layers are formed if the anneal temperature is 850°C.

The electrical activation and carrier mobilities are low in all cases. For doses of 10^{13} and 10^{15} ions/cm^2, raising the implantation temperature from room temperature to 200°C has the effect of improving the n-type electrical activation without causing a conductivity type conversion. The improvement can be as much as a factor of 3 depending on the anneal temperature.

The room temperature implants are characterized by a surface inactive region in which the carrier concentration is very low, and which can be reduced or eliminated by raising the implantation temperature. This suggests that the surface inactive layer is a highly damaged region. The carrier distribution profiles for room temperature implants are shallow (~ 900 Å) and end very abruptly. The corresponding profiles for 200°C implants are more extended (~ 2000 Å) and end more gradually.

Photoluminescence shows that the anneal temperature for maximum lattice recovery is 850°C. However, even for this anneal temperature, a significant amount of residual damage is still present in the lattice, as indicated by the presence of a Ga-vacancy peak in the photoluminescence spectrum. This lends further support for the hypothesis that the surface inactive layers in the implanted regions are highly damaged regions. It also accounts for the low carrier mobilities observed. The Ge-acceptor peak at 1.481 eV has been observed for all implantation and annealing conditions, indicating that the implanted layers are always compensated. Two peaks of unknown origin at 1.432 eV and 1.294 eV have been observed for room temperature 10^{14} ions/cm^2 implants. The peak at 1.432 eV occurs in samples annealed at 850°C. The peak at 1.294 eV is extremely broad and appears in samples annealed at 900°C.

Planar diodes having a Ge-implanted p-side have been fabricated. Reverse breakdown occurs at 50V and is rather soft. The leakage current is ohmic for low reverse bias (< 2V), indicating the presence of a resistive shunt across the junction, most probably due to the highly damaged surface inactive layer in the implanted regions. The forward current is proportional to $\exp(qV/nkT)$, with an anomalous value of n = 6.2.

The data presented in this work suggest that the amphoteric behavior of Ge-implanted GaAs is controlled by complex impurity-defect interactions. Unless ways are found to raise the electrical activation and carrier mobility, and to improve the junction characteristics, the amphoteric property of Ge implanted into GaAs will remain a topic of academic interest only.

REFERENCES

1. C. Constantinescu and I. Petrescu-Prahova, "Acceptor Behavior of Germanium in Gallium Arsenide," J. Phys. Chem. Solids, Vol. 28, pp. 2397-2400, 1967.

2. F. E. Rosztoczy, F. Ermanis, I. Hayashi and B. Schwartz, "Germanium-Doped Gallium Arsenide," J. Appl. Phys., Vol. 41, pp. 264-270, 1970.

3. H. Kressel, F. Z. Hawrylo and P. LeFur, "Luminescence due to Ge Acceptors in GaAs," J. Appl. Phys., Vol. 39, pp. 4059-4066, 1968.

4. W. Schairer and W. Graman, "Photoluminescence of Ge-Doped GaAs Grown by Vapor-Phase Epitaxy," J. Phys. Chem. Solids, Vol. 30, pp. 2225-2229, 1969.

5. A. Y. Cho and I. Hayashi, "P-N Junction Formation during Molecular-Beam Epitaxy of Ge-Doped GaAs," J. Appl. Phys., Vol. 42, pp. 4422-4425, 1971.

6. H. Kasano, "Diatomic-Complex Donor and Acceptor Model for Ge-Doped Vapor-Grown GaAs," J. Appl. Phys., Vol. 49, pp. 4021-4030, 1978.

7. V. M. Zelevinskaya and G. A. Kachurin, "Behavior of Germanium Implanted in GaAs by Ion Bombardment," Sov. Phys. Semicond., Vol. 5, pp. 1011-1013, 1971.

8. J. Lindhard, M. Scharff and H. Schiott, "Range Concepts and Heavy Ion Ranges," Mat. Fys. Medd. Dan. Vid. Selsk., Vol. 33, pp. 1-39, 1963.

9. J. F. Gibbons, W. S. Johnson and S. W. Mylroie, Projected Range Statistics, Semiconductors and Related Materials, 2nd edition. Stroudsburg, Pennsylvania: Dowden, Hutchinson and Ross, 1975.

10. S. T. Picraux, in Ion Implantation in Semiconductors and Other Materials. B. L. Crowder, Editor. New York: Plenum Press, 1973. p. 641.

11. K. V. Vaidyanathan, M. J. Helix, D. J. Wolford, B. G. Streetman, R. J. Blattner and C. A. Evans, Jr., "Study of Encapsulants for Annealing GaAs," J. Electrochem. Soc., Vol. 124, pp. 1781-1784, 1977.

12. M. J. Helix, K. V. Vaidyanathan, B. G. Streetman, H. B. Dietrich and P. K. Chatterjee, "R.F. Plasma Deposition of Silicon Nitride Layers," Thin Solid Films, Vol. 55, pp. 143-148, 1978.

13. L. J. van der Pauw, "A Method of Measuring Specific Resistivity and Hall Effect of Discs of Arbitrary Shape," Philips Res. Repts., Vol. 13, pp. 1-9, 1958.

14. C. J. Nuese and J. J. Gannon, "Silver-Manganese Evaporated Ohmic Contacts to P-type Gallium Arsenide," J. Electrochem. Soc., Vol. 115, pp. 327-328, 1968.

15. W. V. McLevige, P. K. Chatterjee and B. G. Streetman, "Versatile Double A.C. Hall Effect System for Profiling Impurities in Semiconductors," J. Phys. E: Sci. Instrum., Vol. 10, pp. 335-337, 1977.

16. W. V. McLevige, "Annealing Studies of Beryllium in Gallium Arsenide and Gallium Arsenide Phosphide," Ph.D. thesis, U. of Illinois, 1978.

17. D. R. Myers, "Properties of Silicon Implanted with Arsenic through Silicon Dioxide," Ph.D. thesis, U. of Illinois, 1977.

18. M. J. Helix, K. V. Vaidyanathan and B. G. Streetman, "Properties of Be-Implanted Planar GaAs p-n Junctions," IEEE J. Solid-State Circuits, Vol. SC-13, pp. 426-429, 1978.

19. H. B. Bebb and E. W. Williams, "Photoluminescence I: Theory," Semiconductors and Semimetals, Vol. 8, edited by R. K. Willardson and A. C. Beer, New York: Academic Press, 1975. pp. 181-320.

20. E. W. Williams and H. B. Bebb, "Photoluminescence II: GaAs," Semiconductors and Semimetals, Vol. 8, edited by R. K. Willardson and A. C. Beer, New York: Academic Press, 1975. pp. 321-392.

21. M. D. Sturge, "Optical Absorption of GaAs between 0.6 and 2.75 eV," Phys. Rev., Vol. 127, pp. 768-773, 1962.

22. G. T. Marcyk, "Atomic and Electrical Profile Studies of Ion-Implanted Semiconductors," Ph.D. thesis, U. of Illinois, 1978.

23. P. K. Chatterjee, K. V. Vaidyanathan, M. S. Durschlag and B. G. Streetman, "Photoluminescence Study of Native Defects in Annealed GaAs," Solid State Commun., Vol. 17, pp. 1421-1424, 1975.

24. P. K. Chatterjee, K. V. Vaidyanathan, W. V. McLevige and B. G. Streetman, "Photoluminescence from Be-Implanted GaAs," Appl. Phys. Lett., Vol. 27, pp. 567-569, 1975.

25. M. J. Helix, "Encapsulation Studies and Planar Device Fabrication in Gallium Arsenide," Ph.D. thesis, U. of Illinois, 1979.